Sensor Selection, State Estimation and Fault Diagnosis of Simple Rotor-Bearing Systems

by

Rui Pan

A thesis submitted in partial fulfillment of the requirements for the degree of

Master of Science

in

Control Systems

Department of Electrical and Computer Engineering
University of Alberta

Abstract

In this research, state and imbalance fault estimation of a simple rotor-bearing system using Kalman filtering techniques has been investigated. The motion of a simple rotor-bearing system can be described by a set of coupled partial differential equations (PDEs); approximative equations of the motion PDEs are derived by variational formulation, where the PDE system is spatially discretized into a high dimensional ordinary differential equation (ODE) form. Optimization-based sensor selection algorithm for Kalman filtering is then applied to optimally choose among the large number of ODE model states to measure, such that specific requirements for state estimation performance are satisfied with a small number of sensors. For practical applications such as the rotor-bearing systems, fault estimation is usually one of the goals of system monitoring; augmented-state Kalman filter (ASKF) is preferred for its simple formulation, but at the cost of more intensive computation and greater numeric errors due to higher system order. Alternatively, optimal two-stage Kalman filter (OTSKF) provides an equivalent form of ASKF under certain algebraic constraint but with generally lower computation complexity and many practical advantages. Adaptive two-stage Kalman filter (ATSKF) is thus applied in this research for simultaneous state and fault estimation of the rotor-bearing system, and the optimal adaptive fading factor for OTSKF is designed using the innovation sequence which is equivalent to that of ASKF. Simulation results have demonstrated the effectiveness of ATSKF handling sudden imbalance fault occurrence during the operation of the rotor-bearing system using the optimally selected sensors.

Acknowledgements

I would like to express my sincere gratitude to my supervisor, Dr. Qing Zhao, for her continuous contributions to my research journey and personal growth. I would also like to thank Dr. Zhao for all the support and patience during the last two years of the program when I've been dealing with personal and health matters.

My deepest appreciation for all the financial support I have received from: Dr. Qing Zhao for 2013 - 2015, Ian Taylor and Carl Knickerbocker for 2015 - 2016, Curtis Greenland and Michelle Demers for 2016 - current. It is my greatest honor to work with and learn from you.

Contents

List of Figures

List of Tables

List of Abbreviations

AFKF	Adaptive fading Kalman filter
ASKF	Augmented-state Kalman filter
ATSKF	Adaptive two-stage Kalman filter
FE	Finite element
FIM	Fisher Information Matrix
MSE	Mean squared error
ODE	Ordinary differential equation
ODS	Operating deflection shape
OTSKF	Optimal two-stage Kalman filter
PDE	Partial differential equation

Chapter 1

Introduction

1.1 Motivation

Rotating machinery is widely used in all leading industries, and they can vary enormously in size, complexity and general configuration. Unfortunately, there are many causes of machine faults or failures, such as mass unbalance, bent or cracked shafts, and bearing failures [5], which will pose potential damages or interrupt normal operation of the machineries. Moreover, many faults only demonstrate relatively subtle changes in observable vibration signal characteristics until significant damage has occurred. An early detection and diagnosis of these faults can prevent unnecessary interruption of operations and severe damages to the machineries, which can generally lead to huge economic losses. Therefore, modeling and analyzing rotating machines and their fault responses are of great importance for both machine design and operation safety purposes [8].

Motivated by centrifugal separator nozzle plugging issues that commonly present in process industries, this thesis is focused on developing a simple rotor-bearing system model that can simulate the imbalance influence on the normal operation of the machinery, and further designing filtering strategies for simultaneous state and fault estimation. Since recent research on optimal sensor selection in control engineering also fits perfectly in state estimation topics, a study on sensor selection, state and fault diagnosis of simple rotor-bearing systems is of great practical value.

1.2 Literature Review

In this section, a brief overview of existing literatures that are related to structural dynamics modeling and state estimation, sensor selection and Kalman filtering techniques are presented.

1.2.1 State Estimation for Mechanical and Structural Systems

Generally, the equations of motion for mechanical and structural systems can be developed using the Lagrange method or direct Newton's second law of motion [8], and the resulting equations can be ordinary differential equations (ODEs) or partial differential equations (PDEs), coupled or non-coupled, linear or nonlinear. In the case of PDEs, an analytic solution may not be possible to obtain; finite element (FE) discretization are commonly adopted to derive an approximate ODE model that is suitable for simulation, estimation and control design.

A dynamic modeling procedure of rotor-bearing systems, which consist of rigid disks, distributed parameter rotor elements and discrete bearings is presented in [22], the accuracy of the approximate equitations is achieved at the cost of high order system matrices, which may require intensive computation and can lead to large numeric errors. A model reduction technique is proposed in [7] that provides a low order model while retaining the effect of parameter changes and guaranteeing unchanged natural frequency of interest. In [27], modal observer is designed for monitoring the vibration of cantilever model and demonstrates satisfactory results. In a recent paper [19], a robust imbalance fault estimation algorithm is proposed based on an unknown-input observer design method to handle model uncertainty and errors, and satisfactory fault estimation result is obtained. In [9], a second-order natural estimation algorithm is designed for state estimation of a partially instrumented mass-string-damper structure subject to random loads, and the optimal model-based algorithm can provide results close to *Kalman filter*. These literatures suggest that it is efficient to adopt state estimator to monitor vibrations and supervise characteristic parameters of the structure such as eigenfrequencies.

1.2.2 Sensor Selection for Kalman Filtering

The advancement in sensor technology brings industries with affordable sensors to monitor process variables and structure health. Indeed, sensor network and data fusion research offers promising benefits to control and structural engineering, while sensor selection and placement still demonstrate significant advantage in easy computation, lower

cost and suitability in mechanical and structural systems. Especially in monitoring of large scale structures where thousands of sensor locations can be selected [21], optimal sensor placement can significantly reduce the number of target locations to tens or fewer.

Unlike optimal sensor placement in structural engineering [21] and optimal design or inverse problem [3], where Fisher Information Matrix (FIM) is highly relied on, the sensor selection problem for control system engineering focuses on finding relatively small number of measurements to produce satisfactory state estimation solution, and this topic has drawn significant attention in recent years. Minimal controllability problem in [23] outlines an NP-hard algorithm to find the minimal number of states to control to ensure system controllability; the dual problem, minimal observability, can utilize the same strategy to find the minimal number of states to measure so that observability is guaranteed, and observers can be safely designed to monitor system dynamics. Sensor selection for Kalman filtering gains significant amount of attention not only because of the superior ability of Kalman filtering to optimally handle dynamics disturbance and noise, but also the selection can be conducted using state estimation error covariance dynamics that can be calculated offline. [26] points out a few fundamental limitations of sensor selection for optimal Kalman filtering, and that adding new sensors becomes ineffective for reduction of estimation error after the first few, which is one of the most important motivations of performing sensor selection. Most applications [10, 29] focus on improving covariance metrics of certain form, such as trace and log determinate, while the submodularity (or supermodularity) of these metrics may not hold in general. [14] provides a procedure to check sequence submodularity. Due to the fact that optimal sensor selection problem is in general NP-hard, greedy algorithms are commonly adopted with the proposed optimization problem.

1.2.3 Kalman Filtering for Fault Estimation

Kalman filter [15] produces optimal unbiased state estimate for linear Gaussian systems, and its recursive computation is easy to implement; an accurate model of system dynamics and observations is required. Once these assumptions fail, such as occurrence of fault dynamics, the filter will not be optimal and unacceptably large estimation errors may be produced [12].

A natural solution to this issue is adding fault dynamics into the model, and the resulting higher order system may still be optimally estimated, at the cost of more intensive computation and potential higher numeric errors. [6] introduced *optimal two-stage Kalman filter* (OTSKF) to decouple the *augmented-state Kalman filter* (ASKF) into two parallel filters of reduced order. Solutions of OTSKF for random bias are proposed later in [13, 2, 11],

and weaker algebraic constraint imposed makes it easier for real applications. Another approach is Proportional-Integration Kalman filter [4]; however, due to the design complexity of multiple gain matrices, it is not suitable for general systems.

Performance degradation of Kalman filtering occurs when sudden changes exist in system dynamics or measurement model, whether they are modeled or unmodeled. In [28], *adaptive fading Kalman filter* (AFKF) is proposed, where filter innovation covariance is monitored to capture the occurrence of sudden changes, and the forgetting factor is adaptively updated so that the defined criterion function is minimized. OTSKF has the same drawback due to its equivalence to ASKF, thus in [16, 17], adaptive two-stage Kalman filters are proposed for linear and nonlinear systems; while the optimality is not guaranteed since the bias free filter fading factor is calculated based on non-zero mean innovation sequence, and in fact, only bias filter innovation sequence is suitable for designing the fading factor.

1.3 Outline

This section briefly outlines the organization of the rest of this thesis.

In Chapter 2, an approximate ODE model representation of a simple rotor-bearing system is derived given a set of coupled PDEs that describe the shaft motion. Imbalance force model is approximated utilizing the ODE model. Both free and forced lateral responses are simulated to exterminate whether the selected model parameters are appropriate. The ODE model is then implemented in Simulink with a few assumptions, and simulated vibrations are demonstrated.

In Chapter 3, model reduction technique is firstly applied to lower the order of the high dimensional ODE model, and a simpler state-space model is assembled. State estimation model of *Kalman-Bucy filter* is then built in Simulink to simulate both state filtering and error covariance dynamics. Optimization-based sensor selection among the large number of ODE model states are studied, and an approximation algorithm is outlined, aiming at optimally selecting a small number of senors that are able to guarantee the performance of Kalman filtering. Simulations of sensor selection under different practical constraints are demonstrated to indicate a few fundamental limitations of sensor selection problems, and some useful insights on rotor-bearing system monitoring are analyzed.

In Chapter 4, more practical aspects of using Kalman filtering for vibration estimation are studied. Imbalance faults dynamics are considered in system representation, which results in a higher order system. OTSKF is introduced, as an optimal alternative of ASKF in

lower dimension, to handle the intensive computation complexity. Adaptive fading factor algorithm is utilized to deal with the well known degradation issue of conventional Kalman filtering. Simulations on sensor selection of augmented-state system and ATSKF are performed to test the effectiveness of these methods.

In Chapter 5, conclusion of this research is made and a few valuable future work topics are outlined.

Chapter 2

Modeling and Simulation of Simple Rotor-Bearing Systems

2.1 Introduction

The equations of motion for simple rotor-bearing systems can be developed using the Lagrange method or direct Newton's second law of motion [8]. They are coupled partial differential equations (PDEs), to which an analytic solution is in general impossible to obtain. Finite element discretization provides an approximation scheme to spatially discretize the PDEs into a high order ordinary differential equation (ODE) form, so that simulation, estimation and control can be designed using either the continues-time ODEs or further temporally discretized system representations.

This chapter intends to specify the model representation that is applied for analysis and design throughout this thesis, and briefly address finite element discretization of simple rotor-bearing systems when the equations of motion are available. A Simulink model is then built according to the derived ODE representation to simulate the states and measurements of an idealized simple rotor-bearing system. Limitations of the Simulink model are specified. Simulations of free and forced lateral response and vibration measurements are presented to demonstrate the behavior of the model. This chapter serves as the basis for the rest of this thesis.

2.2 Model Description and Preliminaries

2.2.1 Model Description

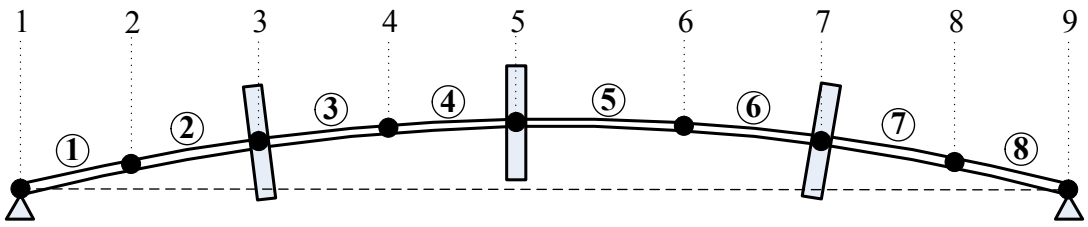

Figure 2.1: A simplified rotor-bearing system model.

The simple rotor-bearing system model of interest in this thesis is consisted of an evenly distributed long-stretched homogeneous and isotropic flexible shaft, three rigid disks, and two isotropic bearings at left and right ends of the shaft, as is demonstrated in Figure 2.1. The partial differential equations describing the motion of such a shaft can be written in the following form [25]:

$$EI_a\frac{\partial^4 u(t,z)}{\partial z^4}+\mu\frac{\partial^2 u(t,z)}{\partial t^2}-I_a\frac{\partial^4 u(t,z)}{\partial t^2\partial z^2}-\omega I_p\frac{\partial^3 v(t,z)}{\partial t\partial z^2}+c\frac{\partial u(t,z)}{\partial t}=0, \tag{2.1a}$$

$$EI_a\frac{\partial^4 v(t,z)}{\partial z^4}+\mu\frac{\partial^2 v(t,z)}{\partial t^2}-I_a\frac{\partial^4 v(t,z)}{\partial t^2\partial z^2}+\omega I_p\frac{\partial^3 u(t,z)}{\partial t\partial z^2}+c\frac{\partial v(t,z)}{\partial t}=0, \tag{2.1b}$$

where t and z are temporal and spatial variables; $u(t,z)$ and $v(t,z)$ are $x-$ and $y-$direction displacements, and the initial conditions of the system are given as $u(0,z)$, $\dot{u}(0,z)$, $v(0,z)$ and $\dot{v}(0,z)$; E, ω and c are defined in Table 2.1, along with the rest of the rotor-bearing system parameter specifications; mess per length μ, diametral and polar moment of inertia of the shaft, I_a and I_p, are calculated as

$$\mu=\rho\pi(\frac{d^s}{2})^2,\ \ I_a=\frac{1}{4}\pi(\frac{d^s}{2})^4,\ \ I_p=\frac{1}{2}\pi(\frac{d^s}{2})^4.$$

In this thesis, shaft motion in Equation (2.1) is the focus of the study on simple rotor-bearing systems since effects of disks and bearings can be modeled as point forces and moments applied on the shaft, and further regarded as boundary or transmission conditions to Equation (2.1), which are briefly demonstrated in the following subsection. Thus, all states and measurements mentioned in the rest of this thesis are with regard to the shaft motions. Note that gravity effects are ignored in this model for simplicity, and one practical application of such a setup is centrifuge machine [19].

Table 2.1: Model Parameter Specification

	Parameter	Symbol	Value
System	External viscous damping factor	c	0 Ns/m
	Spinning speed	ω	1000 RPM
Shaft	Length	L	1.5 m
	Diameter	d^s	50 mm
	Young's modulus	E	2.11×10^{11}N/m^2
	Mass per m^3	ρ	7810 kg/m^3
Disk	Thickness($j = 1,2,3$)	l_j^d	70 mm
	Diameter	d_j^d	280 mm
Bearing	Isotropic bearing damping	c_{uu}^b, c_{vv}^b	0 Ns/m
		c_{uv}^b, c_{vu}^b	0 Ns/m
	Isotropic bearing stiffness	k_{uu}^b, k_{vv}^b	1×10^6 N/m
		k_{uv}^b, k_{vu}^b	0 N/m

2.2.2 Finite Element Discretization

Spatial Discretization

Assume the system model demonstrated in Figure 2.1 can be discretized into N finite elements with $N+1$ nodes $\{z_k\}_{i=1}^{N+1}$ (z_1 and z_{N+1} are bearing nodes). For an element bounded by nodes z_k and z_{k+1}, apply standard 3rd order Hermite polynomials (also called shape function) $\left\{\Psi_p^k(z)\right\}_{p=1}^4$ to derive the approximative displacement in $z \in [z_k, z_{k+1}]$ as

$$u(t,z)|_{z\in[z_k,z_{k+1}]} = \Psi_1^k(z)u_k(t) + \Psi_2^k(z)\gamma_k(t) + \Psi_3^k(z)u_{k+1}(t) + \Psi_4^k(z)\gamma_{k+1}(t),$$
$$v(t,z)|_{z\in[z_k,z_{k+1}]} = \Psi_1^k(z)v_k(t) - \Psi_2^k(z)\beta_k(t) + \Psi_3^k(z)v_{k+1}(t) - \Psi_4^k(z)\beta_{k+1}(t),$$

where $u_k(t)$, $v_k(t)$, $\beta_k(t)$ and $\gamma_k(t)$ are the $x-$ and $y-$direction displacements and $Ox-$ and $Oy-$direction angles at z_k. Denote $q_k(t) = [u_k(t)\ v_k(t)\ \beta_k(t)\ \gamma_k(t)]^\top$, $\tilde{q}_k(t) = [q_k^\top(t)\ q_{k+1}^\top(t)]^\top$ and $U(t,z) = [u(t,z)\ v(t,z)]^\top$, then

$$U(t,z)_{|z\in[z_k,z_{k+1}]} = W_k(z)\tilde{q}_k(t), \tag{2.2}$$

where

$$W_k(z) = \begin{bmatrix} \Psi_1^k(z) & 0 & 0 & \Psi_2^k(z) & \Psi_3^k(z) & 0 & 0 & \Psi_4^k(z) \\ 0 & \Psi_1^k(z) & -\Psi_2^k(z) & 0 & 0 & \Psi_3^k(z) & -\Psi_4^k(z) & 0 \end{bmatrix}. \quad (2.3)$$

Figure 2.2 demonstrates the values of Hermite polynomials and their derivatives for element bounded by $[z_4, z_5]$. As is indicated, at $z = z_k$, only $\Psi_1^k(z)$ and $\dot{\Psi}_2^k(z)$ have value 1, which

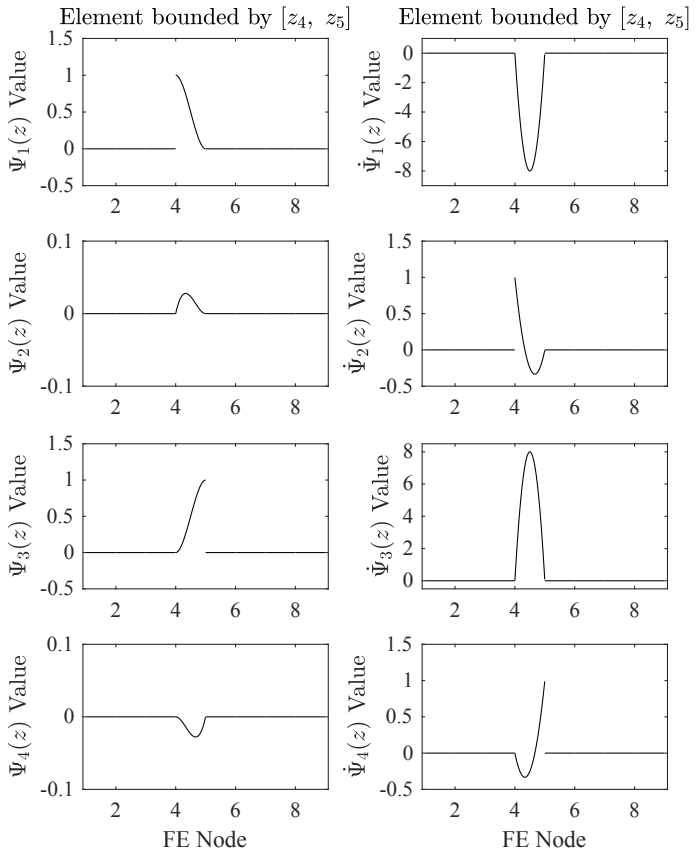

Figure 2.2: Shape function for element bounded by $[z_4, z_5]$.

indicates

$$u(t,z)|_{z=z_k} = u_k(t),\ \ \frac{\partial u(t,z)}{\partial z}|_{z=z_k} = \gamma_k(t),\ \ v(t,z)|_{z=z_k} = v_k(t),\ \ \frac{\partial v(t,z)}{\partial z}|_{z=z_k} = -\beta_k(t).$$

Similar observation can be obtained at $z = z_{k+1}$ as

$$u(t,z)|_{z=z_{k+1}} = u_{k+1}(t),\ \ \frac{\partial u(t,z)}{\partial z}|_{z=z_{k+1}} = \gamma_{k+1}(t),$$
$$v(t,z)|_{z=z_{k+1}} = v_{k+1}(t),\ \ \frac{\partial v(t,z)}{\partial z}|_{z=z_{k+1}} = -\beta_{k+1}(t).$$

In order to assemble the complete system, the displacement and angle vector of the entire shaft can be constructed as

$$\begin{aligned} q(t) &= [q_1^\top(t) \ \cdots \ q_{N+1}^\top(t)]^\top \\ &= [u_1(t) \ v_1(t) \ \beta_1(t) \ \gamma_1(t) \ \cdots \ u_{N+1}(t) \ v_{N+1}(t) \ \beta_{N+1}(t) \ \gamma_{N+1}(t)]^\top, \end{aligned} \tag{2.4}$$

and thus, $\tilde{q}_k(t) = T_k q(t)$, where element assembling matrix T_k is defined as

$$T_k = [\ \mathbf{0}_{8\times 4(k-1)} \ \ \boldsymbol{I}_{8\times 8} \ \ \mathbf{0}_{8\times 4(N-k)}\ ] \in \boldsymbol{R}^{8\times 4(N+1)}.$$

Therefore, Equation (2.2) is equivalent to

$$U(t,z)_{|z\in[z_k,z_{k+1}]} = W_k(z) T_k q(t), \tag{2.5}$$

and the approximative displacement of the entire shaft can be described as following:

$$U(t,z) = \sum_{k=1}^{N} W_k(z) T_k q(t), \tag{2.6}$$

where $\sum_{k=1}^{N} W_k(z) T_k$ is a shape matrix that is only related to spatial variable z, and $q(t)$ is the time dependent coefficients.

Galerkin Formulation

The boundary and transmission conditions at $z_k \in \Omega = [0, L]$ are defined as

$$\left[I_a \ddot{u}' + \omega I_p \dot{v}' - E I_a u'''\right]_{z_k} = f_{z_k,1} \tag{2.7a}$$

$$\left[I_a \ddot{v}' + \omega I_p \dot{u}' - E I_a v'''\right]_{z_k} = f_{z_k,2} \tag{2.7b}$$

$$\left[E I_a u''\right]_{z_k} = t_{z_k,1} \tag{2.7c}$$

$$\left[E I_a v''\right]_{z_k} = t_{z_k,2}, \tag{2.7d}$$

where $'$ is partial derivative with respect to z and $\dot{}$ with respect to t; $[f]_z = f(z^+) - f(z^-)$ denotes the jump of f at z; $f_{z_k,\cdot}$ and $t_{z_k,\cdot}$ are point force and moment occurred at node z_k. When analyzing each element, $f_{z_k,\cdot}$ and $t_{z_k,\cdot}$ include both internal forces and moments and those caused by bearings and disks. The weak solution to Equation 2.1 on Hilbert space can be formulated using Galerkin's method as:

$$\left\langle E I_a u'''' + \mu \ddot{u} - I_a \ddot{u}'' - \omega I_p \dot{v}'' + c\dot{u}, \eta \right\rangle = \langle 0, \eta \rangle,$$

$$\left\langle E I_a v'''' + \mu \ddot{v} - I_a \ddot{v}'' + \omega I_p \dot{u}'' + c\dot{v}, \xi \right\rangle = \langle 0, \xi \rangle,$$

where $\eta, \xi \in H^2(\Omega)$ are test functions. Integrating by parts over $\Omega = [0, L]$ will lead to the variational formulation as

$$\begin{aligned}
&\int_\Omega EI_a u''\eta'' + \mu\ddot{u}\eta + I_a\ddot{u}'\eta' + \omega I_p\dot{v}'\eta' + c\dot{u}\eta \ \mathrm{d}z \\
&\qquad + \sum_{k=1}^{N} \left[EI_a u'''\eta - EI_a u''\eta' - I_a\ddot{u}'\eta - \omega I_p\dot{v}'\eta \right] |_{z_k}^{z_{k+1}} = 0 \\
&\int_\Omega EI_a v''\xi'' + \mu\ddot{v}\xi + I_a\ddot{v}'\xi' - \omega I_p\ddot{u}'\xi' + c\dot{v}\xi \ \mathrm{d}z \\
&\qquad + \sum_{k=1}^{N} \left[EI_a v'''\xi - EI_a v''\xi' - I_a\ddot{v}'\xi + \omega I_p\ddot{u}'\xi \right] |_{z_k}^{z_{k+1}} = 0,
\end{aligned}$$

where $[f]|_{z_k}^{z_{k+1}} = f(z_{k+1}) - f(z_k)$. Note that the summation terms are closely related to Equation (2.7); replacing the summation terms with corresponding boundary and transmission forces and moments, and denoting $W = [\eta \ \xi]^\top$, then adding these two equations yields the following equation:

$$\begin{aligned}
&\int_\Omega \mu W^\top\ddot{U} + I_a(W')^\top\ddot{U}' + cW^\top\dot{U} + (W')^\top \begin{bmatrix} & \omega I_p \\ -\omega I_p & \end{bmatrix} \dot{U}' + EI_a(W'')^\top U'' \ \mathrm{d}z \\
&\qquad + \sum_{k=1}^{N+1} \left\{ [W(z_k)]^\top \begin{bmatrix} f_{z_k,1} \\ f_{z_k,2} \end{bmatrix} + \left[W'(z_k)\right]^\top \begin{bmatrix} t_{z_k,1} \\ t_{z_k,2} \end{bmatrix} \right\} = 0.
\end{aligned} \tag{2.8}$$

According to [25], the shape matrix $\sum_{k=1}^{N} W_k(z)T_k$ can be used as an approximation of W in finite dimensional space $V_{4N} \times V_{4N}$, where finite dimensional subspace $V_{4N} \subset H^2(\Omega)$ has a basis $\{\Psi_p^k\}_{p=1,\ldots,4,k=1,\ldots N}$. Thus, Equation (2.8) is approximated by

$$\begin{aligned}
&\sum_{k=1}^{N} T_k^\top \int_\Omega \mu W_k^\top W_k T_k\ddot{q}(t) + I_a W_k'^\top W_k' T_k\ddot{q}(t) + cW_k^\top W_k T_k\dot{q}(t) + EI_a W_k''^\top W_k'' T_k q(t) \\
&\qquad + \omega I_p W_k'^\top \begin{bmatrix} & 1 \\ -1 & \end{bmatrix} W_k' T_k\dot{q}(t) \ \mathrm{d}z + F^d(t) + F^b(t) = 0,
\end{aligned}$$

where vector $F^d(t)$ and $F^b(t)$ describe the point forces and moments components exerted by rigid disks and bearings; all internal forces and moments cancel each other. The above formulation can be further simplified into

$$M^s\ddot{q}(t) + \omega G^s\dot{q}(t) + C^s\dot{q}(t) + K^s q(t) + F^d(t) + F^b(t) = 0, \tag{2.9}$$

where

$$
\begin{aligned}
M^s &= \sum_{k=1}^{N} T_k^\top \left[\int_\Omega \mu W_k^\top W_k + I_a W_k'^\top W_k' \, \mathrm{d}z \right] T_k, \\
G^s &= \sum_{k=1}^{N} T_k^\top \left[\int_\Omega I_p W_k'^\top \begin{bmatrix} & 1 \\ -1 & \end{bmatrix} W_k' \, \mathrm{d}z \right] T_k, \\
C^s &= \sum_{k=1}^{N} T_k^\top \left[\int_\Omega c W_k^\top W_k \, \mathrm{d}z \right] T_k, \\
K^s &= \sum_{k=1}^{N} T_k^\top \left[\int_\Omega E I_a W_k''^\top W_k'' \, \mathrm{d}z \right] T_k,
\end{aligned}
$$

are mass, gyroscopic, damping and stiffness matrix, respectively.

Disk Components

Assume disks are rigid and can only be mounted at pre-defined nodes $z_k \in (0, L)$. The partial differential equations describing the disk motion can be obtained using Lagrangian method, and their ODE representation be formulated as following:

$$
F_k^d(t) = M_k^d \ddot{q}_k(t) + \omega G_k^d \dot{q}_k(t) + C_k^d \dot{q}_k(t), \tag{2.10}
$$

where

$$
M_k^d = \begin{bmatrix} m_d & 0 & 0 & 0 \\ 0 & m_d & 0 & 0 \\ 0 & 0 & I_a^d & 0 \\ 0 & 0 & 0 & I_a^d \end{bmatrix}, \quad G_k^d = \begin{bmatrix} 0 & 0 & 0 & 0 \\ 0 & 0 & 0 & 0 \\ 0 & 0 & 0 & I_p^d \\ 0 & 0 & -I_p^d & 0 \end{bmatrix}, \quad C_k^d = \begin{bmatrix} c & 0 & 0 & 0 \\ 0 & c & 0 & 0 \\ 0 & 0 & 0 & 0 \\ 0 & 0 & 0 & 0 \end{bmatrix};
$$

m_d, I_a^d and I_p^d are disk mass, diametral and polar moment of inertia of the disk calculated as [8]:

$$
m_d = \frac{1}{4}\rho\pi l^d \left[(d^d)^2 - (d^s)^2 \right], \quad I_p^d = \frac{1}{8} m_d \left[(d^d)^2 + (d^s)^2 \right], \quad I_a^d = \frac{1}{2} I_p^d + \frac{1}{12} m_d (l^d)^2.
$$

Define disk assembling matrix T_k^d, $k = 2, 3, \cdots, N$ as following:

$$
T_k^d = \begin{cases} [\, \mathbf{0}_{4\times 4(k-1)} \;\; \boldsymbol{I}_{4\times 4} \;\; \mathbf{0}_{4\times 4(N-k+1)} \,] \in \boldsymbol{R}^{4\times 4(N+1)} & \text{if a disk is mounted at node } k \\ \mathbf{0}_{4\times 4(N+1)} \in \boldsymbol{R}^{4\times 4(N+1)} & \text{if no disk is mounted at node } k, \end{cases}
$$

and $q_k(t) = T_k^d q(t)$. Thus,

$$F^d(t) = M^d \ddot{q}(t) + \omega G^d \dot{q}(t) + C^d \dot{q}(t), \tag{2.11}$$

where

$$M^d = \sum_{k=2}^{N} (T_k^d)^\top M_k^d T_k^d, \;\; G^d = \sum_{k=2}^{N} (T_k^d)^\top G_k^d T_k^d, \;\; C^d = \sum_{k=2}^{N} (T_k^d)^\top C^d T_k^d.$$

Remark 2.2.1 *It should be pointed out that this formation is identical with Equation (2.8), because when $W(z_k)$ and $W'(z_k)$ are approximated using $W_k(z_k)$ and $W_k'(z_k)$, only two entries of each matrix are non-zero value according to Figure 2.2, and the combined influence is equivalent to T_k^d. Same conclusion can be made for bearing effects that are modeled as boundary conditions.*

Bearing Components

It is assumed that two bearings are mounted at the both ends of the shaft to support it. Assume the bearings utilized obey the following governing equations:

$$C_k^b \dot{q}_k(t) + K_k^b q_k(t) = F_k^b(t), \tag{2.12}$$

where $k = 1$ or $N+1$, and

$$C_k^b = \begin{bmatrix} c_{uu}^b & c_{uv}^b & 0 & 0 \\ c_{vu}^b & c_{vv}^b & 0 & 0 \\ 0 & 0 & 0 & 0 \\ 0 & 0 & 0 & 0 \end{bmatrix}, \;\; K_k^b = \begin{bmatrix} k_{uu}^b & k_{uv}^b & 0 & 0 \\ k_{vu}^b & k_{vv}^b & 0 & 0 \\ 0 & 0 & 0 & 0 \\ 0 & 0 & 0 & 0 \end{bmatrix}.$$

Define assembly matrix

$$T_k^b = \begin{cases} [\boldsymbol{I}_{4\times4} \; \boldsymbol{0}_{4\times4N}] \in \boldsymbol{R}^{4\times4(N+1)} & \text{if } k = 1; \\ [\boldsymbol{0}_{4\times4N} \; \boldsymbol{I}_{4\times4}] \in \boldsymbol{R}^{4\times4(N+1)} & \text{if } k = N+1; \end{cases}$$

and then,

$$F^b(t) = C^b \dot{q}(t) + K^b q(t), \tag{2.13}$$

where

$$C^b = (T_1^b)^\top C_1^b T_1^d + (T_{N+1}^b)^\top C_{N+1}^b T_{N+1}^d, \;\; K^b = (T_1^b)^\top K_1^b T_1^d + (T_{N+1}^b)^\top K_{N+1}^b T_{N+1}^d.$$

System Assembly

The overall system equation is obtained by substituting Equation (2.11) and (2.13) into Equation (2.9), as the following form:

$$M^{fe}\ddot{q}(t) + \omega G^{fe}\dot{q}(t) + C^{fe}\dot{q}(t) + K^{fe}q(t) = 0, \tag{2.14}$$

where

$$M^{fe} = M^s + M^d,\ \ G^{fe} = G^s + G^d,\ \ C^{fe} = C^s + C^d + C^b,\ \ K^{fe} = K^s + K^b,$$

and M^{fe}, G^{fe}, C^{fe}, $K^{fe} \in \boldsymbol{R}^{4(N+1)\times 4(N+1)}$, $q(t) \in \boldsymbol{R}^{4(N+1)}$.

Imbalance Fault Components

In this research, only imbalance forces are considered for the fault scenario. Let vector $q_\varepsilon(t) \in \boldsymbol{R}^{4(N+1)}$ be the difference between equilibrium position and rotor center of mass at all modeled nodes along the shaft, and the new system equation with imbalance fault can be formulated as [8]:

$$M^{fe}[\ddot{q}(t) + \ddot{q}_\varepsilon(t)] + \omega G^{fe}[\dot{q}(t) + \dot{q}_\varepsilon(t)] + C^{fe}\dot{q}(t) + K^{fe}q(t) = 0. \tag{2.15}$$

Since excitation and response are harmonic, $\ddot{q}_\varepsilon(t) = -\omega^2 q_\varepsilon(t)$. Therefore, imbalance fault signal can be formulated as

$$f_{\text{im}}(t) = -M^{fe}\ddot{q}_\varepsilon(t) - \omega G^{fe}\dot{q}_\varepsilon(t) = \omega^2 M^{fe} q_\varepsilon - \omega G^{fe}\dot{q}_\varepsilon. \tag{2.16}$$

Due to the fact that disk masses are significantly greater than shaft elements, it is reasonable to assume imbalance forces can only appear on disks, namely,

$$f_{\text{im}}(t) = F_0 f(t), \tag{2.17}$$

where $F_0 \in \boldsymbol{R}^{4(N+1)\times 4N^d}$ represents the imbalance fault model, N^d is disk number; $f(t) \in \boldsymbol{R}^{4N^d}$ is assumed to share the same physical meaning with imbalance position $q_\varepsilon(t)$ but only at nodes where disks are mounted. For a specific disk node $z_k \in (0, L)$, let

$$q_{\varepsilon,k} = [\varepsilon_k \cos(\omega t + \delta_k), \varepsilon_k \sin(\omega t + \delta_k), 0, 0]^\top,\ M^{fe}_{z_k} = M^d_k,\ G^{fe}_{z_k} = G^d_k,$$

where ε_k is the magnitude or imbalance position from the equilibrium, and δ_j is the phase, and then,

$$[F_0 f(t)]_k = \omega^2 \left[m^d \varepsilon_k \cos(\omega t + \delta_j), m^d \varepsilon_k \sin(\omega t + \delta_j), 0, 0\right]^\top. \tag{2.18}$$

To conclude, the ODE representation of the simple rotor-bearing system using finite element discretization under imbalance forces can be written as:

$$M^{fe}\ddot{q}(t) + \omega G^{fe}\dot{q}(t) + C^{fe}\dot{q}(t) + K^{fe}q(t) = F_0 f(t) + D_0 w(t), \tag{2.19}$$

where D_0 and $w(t)$ are to represent the modeling error or system disturbance. For simplicity reason, damping factor is not considered (as is defined in Table 2.1, $c = 0$) in analysis and simulation of this research, thus the damping C^{fe} matrix term is ignored in the rest of this thesis. It is worthwhile pointing out that doing this will lead to pure imaginary eigenvalues of the system.

2.3 Simulation Results and Discussions

In this section, various simulation results using parameters described in Table 2.1 are presented, which is based on 8 (value of N) evenly discretized elements, 3 disks and 2 bearings. The main goal of the simulation is to achieve comprehensive understanding of the rotor-bearing system of interest before applying advanced algorithms for sensor selection and state estimation.

2.3.1 Free Lateral Response

Recall the homogeneous form of the ODE model of shaft motion in Equation (2.14), neglecting damping terms, as:

$$M^{fe}\ddot{q}(t) + \omega G^{fe}\dot{q}(t) + K^{fe}q(t) = 0.$$

Table 2.2: Rotor-bearing system eigenvalues at spinning speed 1000 RPM

Backward Whirl	Forward Whirl
$5.8318 \times 10^{-12} \pm 83.9083i$	$-8.4590 \times 10^{-12} \pm 84.5805i$
$4.3826 \times 10^{-11} \pm 237.7725i$	$-4.1020 \times 10^{-11} \pm 244.1232i$
$1.9806 \times 10^{-12} \pm 537.8319i$	$-1.9877 \times 10^{-12} \pm 563.7432i$
$-1.0026 \times 10^{-12} \pm 1131.6896i$	$6.5512 \times 10^{-12} \pm 1199.2507i$

The roots of the characteristic equation are in form of $s_1, s_2 = -\zeta\omega_n \pm j\omega_n\sqrt{1-\zeta^2}$. Since no damping has been considered, $\zeta = 0$, and the roots are expected to be pure imaginary. At rotor spinning speed of 1000 RPM, the first four sets of eigenvalues of both backward and forward whirls are listed in Table 2.2, and the extremely small non-zero real parts are due to numeric errors. The corresponding first four natural frequencies and mode shapes are demonstrated in Figure 2.3, where the natural frequencies are calculated as $1/(2\pi)$ of the imaginary parts of corresponding backward whirl eigenvalues.

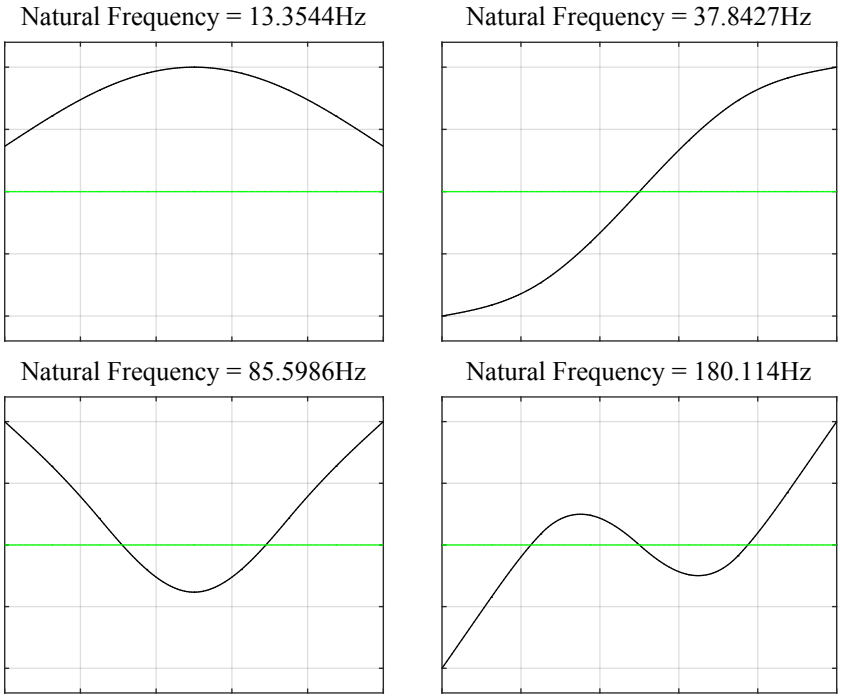

Figure 2.3: Rotor-bearing system first four mode shapes.

Further, the natural frequency map is illustrated in Figure 2.4, where a larger range of spinning speeds are taken into consideration. It presents computed values of natural frequencies as a function of rotor rotation speed. The intersection of 1x natural frequency function (blue dash line) with calculated natural frequency (black lines with red and greed markers) around 800 RPM indicates a critical speed at the low speed range, around where rotor imbalance produces unacceptable vibrations. In this thesis, the system spinning speed is chosen to be 1000 RPM, which is above this critical speed and thus safe for operation.

To conclude, free lateral response is analyzed in the absence of any applied forces. Thus, the vibration response indicates system properties, and can be used for design and

model parameter validation.

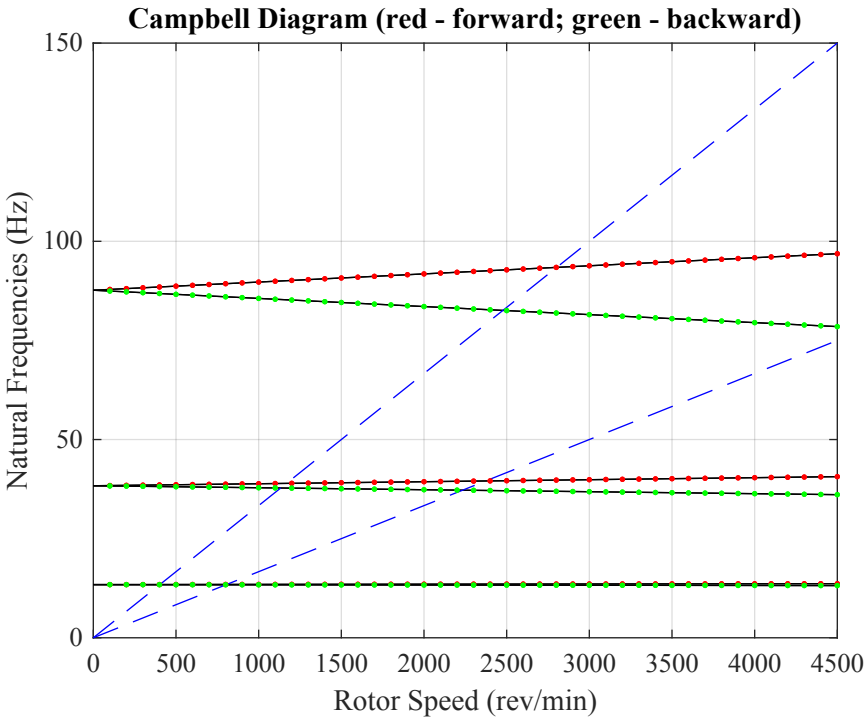

Figure 2.4: Rotor-bearing system Campbell diagram.

2.3.2 Forced Lateral Response

Assume that the steady-state forced response of system described by Equation (2.19) (with no damping component or modeling error, namely, $C^{fe} = 0$ and $D_0 w(t) \equiv 0$) has the form of $q(t) = \mathbf{Re}(q_0(t)\mathrm{e}^{j\omega t})$, where $\mathbf{Re}(\cdot)$ represents the real part. Thus,

$$q_0(t) = [(K^{fe} - \omega^2 M^{fe}) + j\omega(\omega G^{fe})]^{-1} \cdot F_0 f(t). \tag{2.20}$$

Figure 2.5 and 2.6 demonstrate the steady-state response of rotor-bearing system with an imbalance mass eccentricity of 10mm at node 3. It is noticeable that when the synchronized imbalance fault excitation approaches natural frequency of the system, the magnitude of the response reaches a local maximal; the imbalance force also leads to a significant small value in magnitude of node 3 around 1600 RPM, and the phase of the node changes by 180°. This observation is more clearly demonstrated in Figure 2.6.

Thus, forced lateral response is very helpful for analyzing the behavior of system under applied forces. Through various figures that can be produced using the forced steady-state response, a preliminary understanding of system response can be established.

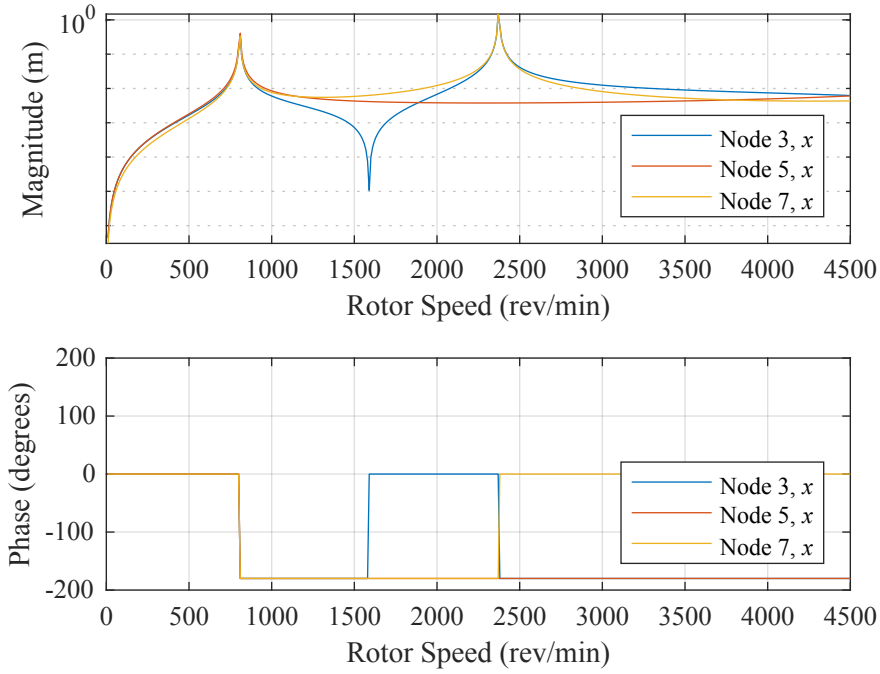

Figure 2.5: Steady-state response of system with an imbalance placed in node 3.

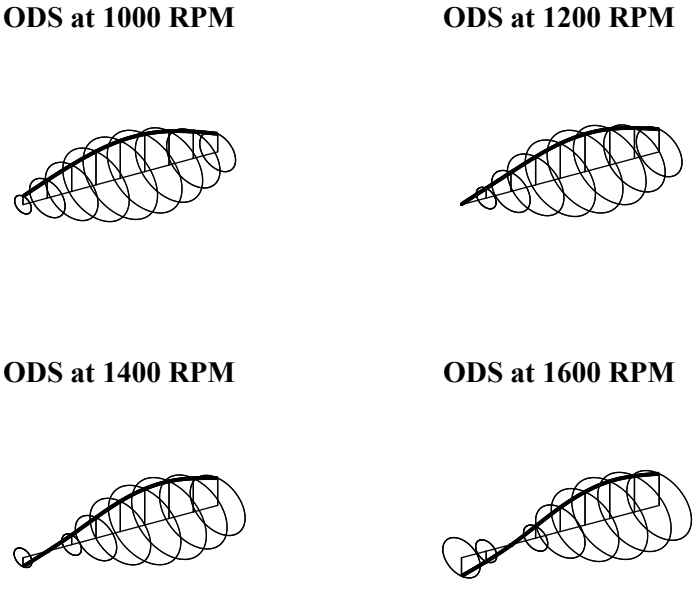

Figure 2.6: Steady-state ODS of system with an imbalance placed in node 3.

2.3.3 Simulation Model Limitations

Given the approximate ODE representation of the rotor-bearing system, the simulation performed in this thesis is regarding the rotor-bearing system as an second-order ordinary differential equation system, unlike simulations performed in mechanical or structural dynamics analysis softwares, such as SimMechanics and Ansys [19], where the physical characteristics are heavily emphasized. Therefore, a few limitations are associated with the simulation model used in this thesis, mainly due to lack of constant control inputs. A few clarifications are required to be presented.

- **Initial conditions**: Since control inputs are not designed for the model, the simulations heavily rely on initial conditions (or equivalently, impulse input), while an accurate initial condition is difficult to obtain in this case. In this thesis, the initial condition is chosen by assuming a known small imbalance at the middle disk, and then the steady-state response with respect to this known imbalance is calculated to be used as initial condition to excite the system. Due to lack of constant excitation and damping force, the system will oscillate at natural frequency.

- **Imbalance Fault Excitation**: Since the initial condition driven system operates at natural frequency rather than the designed spinning speed, the imbalance fault excitation modeled following Equation (2.16) is not synchronized with the system anymore. However, simulation under this asynchronized fault signal is still performed, but state and fault estimation falls into more general harmonic fault scenario. From implementation perspective, applying the asynchronized fault can simulate dynamics of the occurrence of the faults. To compensate for this limitation, a second simulation study using forced steady-state response data under imbalance is also presented, where the occurrence of imbalance fault is not captured in the collected data. The combined simulation results shall provide more comprehensive insights of the research topic in this thesis.

2.3.4 System Simulation

According to Equation (2.19), a second-order Simulink model is presented in Figure 2.7. While control input is imposed in the Simulink model, no actual signals are applied.

Figure 2.8 further demonstrates the rotor rotation shapes before and after a static imbalance fault is triggered at Node 3. It can be observed that the imbalance will not only increase the operating deflection shape (ODS) magnitude in general, but also alter the symmetric property of the original system. This observation coincides with Figure 2.6.

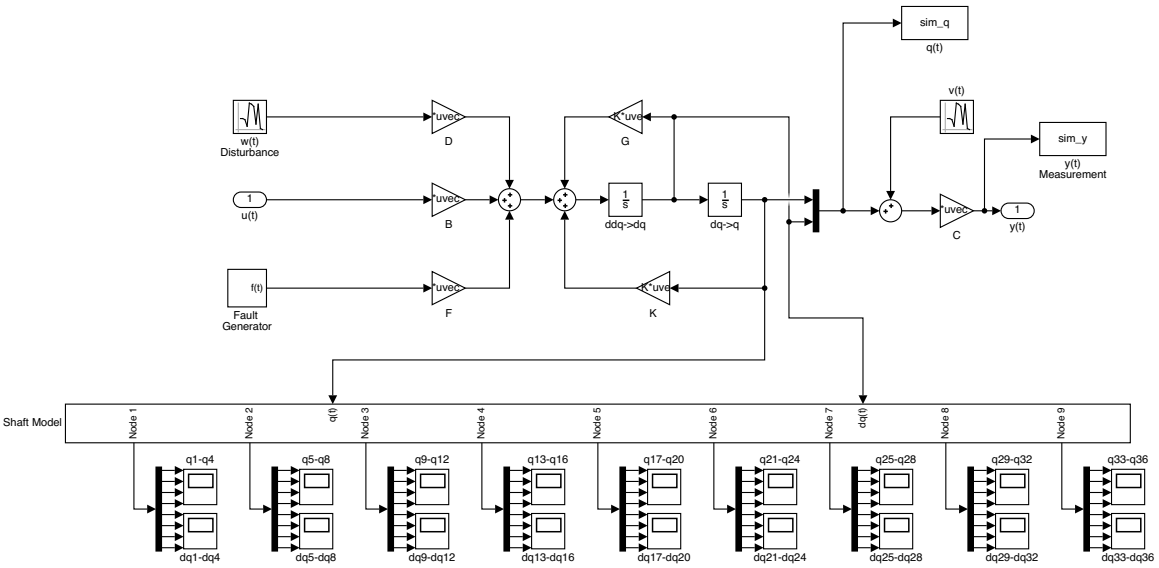

Figure 2.7: Rotor-bearing system Simulink model.

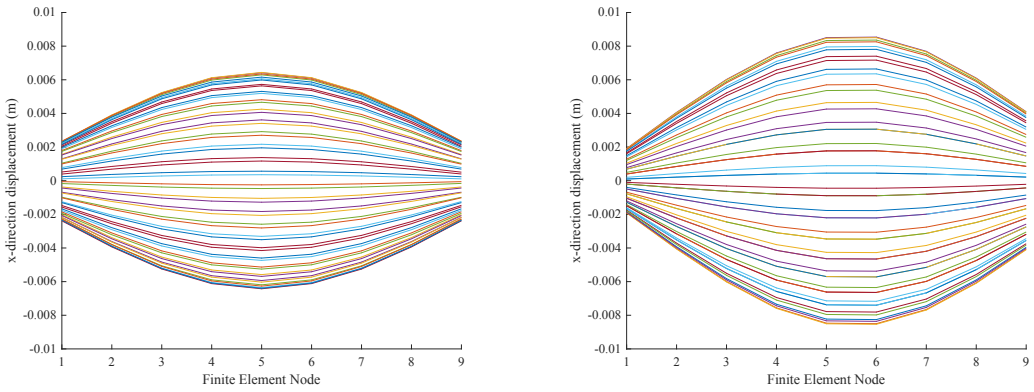

Figure 2.8: Shaft rotation shapes comparison: left: normal condition; right: imbalance fault on node 3.

The rotation shapes under general harmonic fault influence is presented in Figure (2.9). Due to the frequency difference between system oscillation and fault excitation, Figure (2.9) exhibits the phenomenon of beats [24]. Measurement samples from both simulation strategies are presented in Figure 2.10 and 2.11.

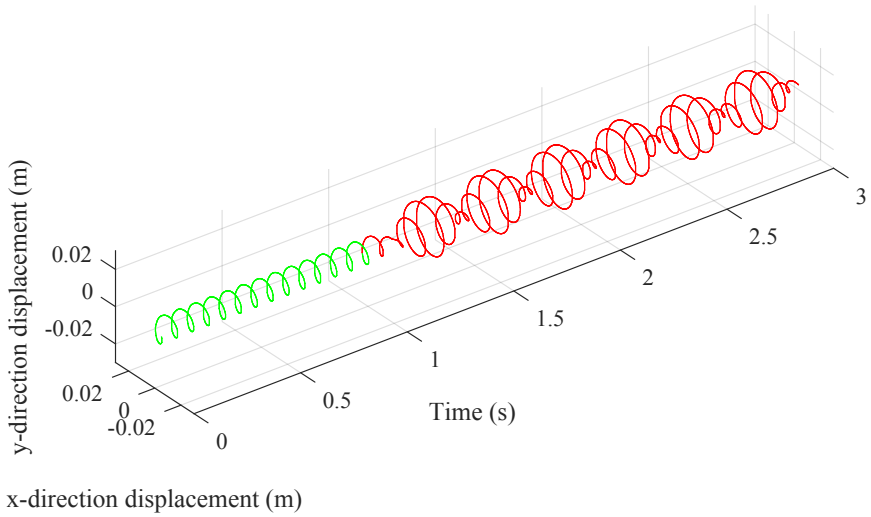

Figure 2.9: Central node rotation shapes comparison: green: normal condition; red: general harmonic fault on node 3

2.3.5 Conclusion

This chapter outlines the model that is studied in this thesis. A Simulink model is designed based on the derived ODE model, and it is used to generate data, such as system outputs, for state and fault estimation in later chapters. While there are limitations associated with the setup, a combinational simulation strategy is designed to provide more comprehensive results.

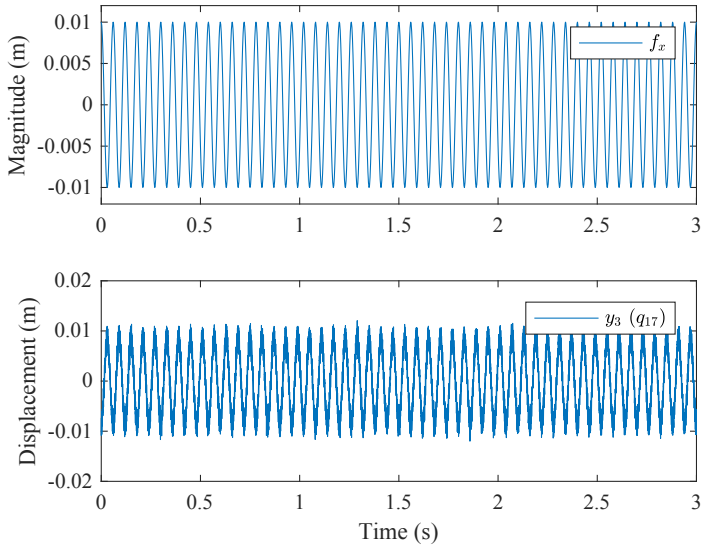

Figure 2.10: Measurement sample from center node x-direction displacement when imbalance fault is applied.

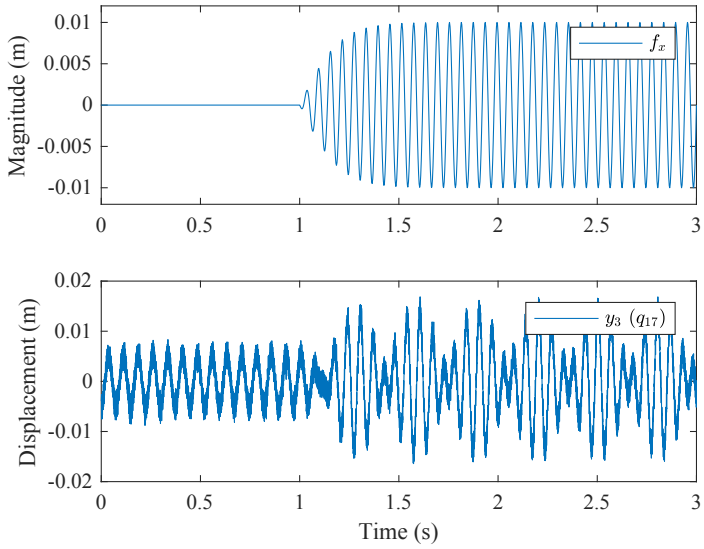

Figure 2.11: Measurement sample from center node x-direction displacement when general harmonic imbalance fault is applied.

Chapter 3

Sensor Selection for Kalman Filtering

3.1 Introduction

Chapter 2 outlines finite element discretization based on partial differential equation representation of a simple rotor-bearing system. The derived ODE model is usually of very high dimension to ensure the approximation accuracy. Generally, in order to perform model-based state estimation for PDE systems, a state-space representation of the system is formulated based on the ODE model matrices; measurements are collected directly (displacement and velocity) or indirectly (acceleration) from this large set of states for estimation, thus, with or without any kind of reduction techniques, the number of potential sensor combinations are dramatically large.

Sensor selection research focuses on finding adequate amount of sensors or measurements to generate satisfactory state estimation results. It is a very practical subject for real world scenarios where high dimensional approximate ODE models are usually applied: too few sensors will not guarantee system observability or state recovery ability, due to already high system order; too many sensors will not only lead to high cost, but also high computation complexity; even the same amount of sensors, different combinations can provide different qualities of estimates.

In this chapter, optimization-based sensor selection for optimal Kalman filtering is studied. The advantage of Kalman filtering scheme is that the state estimation error covariance dynamics can be calculated (steady-state case) or simulated (conventional case) before any measurements are collected. Even though optimal sensor selection problem is NP-hard by nature, approximation algorithms can be designed to ease the computation. The rest of this chapter is organized as following: a state-space model is first formulated; model reduction

technique is applied to derive a lower dimensional representation for the implementation of *Kalman-Bucy filter*; optimization-based sensor selection problem and approximation algorithm are presented based on Kalman filtering state estimation error covariance dynamics; simulation with respect to various practical limitations are presented to demonstrate the effectiveness of the algorithm; state estimation results are then presented with the selected sensors.

3.2 State Estimation via Kalman Filtering

3.2.1 Model Reduction

Recall homogeneous system representation in Equation (2.14). Since K^{fe} is symmetric given the system assumptions, a pseudo-modal subspace can be formulated by solving eigen-problem $M^{fe}\ddot{q}(t)+K^{fe}q(t)=0$ [7]. Consider the first n_r modes of the eigenvector, and denote the basis as

$$\Phi=[\phi_1\ \cdots\ \phi_{n_r}]\in \boldsymbol{R}^{4(N+1)\times n_r}, \tag{3.1}$$

the mode coordinates $z(t)$ can be constructed as following

$$q(t)=\Phi z(t). \tag{3.2}$$

$z(t)$ shall be separated from spatial variable z or z_k applied in Chapter 2 that $z(t)$ is a time-varying signal. The original system Equation (2.19) of order $2(N+1)$ can then be projected into the pseudo-modal subspace spanned by Φ as a model of order n_r as following:

$$\ddot{z}(t)+\omega G_{n_r}\dot{z}(t)+K_{n_r}z(t)=F_{n_r}f(t)+D_{n_r}w(t) \tag{3.3}$$

where

$$M_{n_r}=\Phi^\top M^{fe}\Phi,\quad G_{n_r}=M_{n_r}^{-1}\Phi^\top G^{fe}\Phi,\quad K_{n_r}=M_{n_r}^{-1}\Phi^\top K^{fe}\Phi,$$
$$F_{n_r}=M_{n_r}^{-1}\Phi^\top F_0,\ \ D_{n_r}=M_{n_r}^{-1}\Phi^\top D_0.$$

3.2.2 State Space Model and Kalman Filtering

In this thesis, assume only direct measurements of the ODE model states are taken into consideration, namely, given a general measurement model as

$$y(t)=C_0q(t)+Gf(t)+v(t)=C_{n_r}z(t)+Gf(t)+v(t), \tag{3.4}$$

where $C_0 \in \boldsymbol{R}^{m\times 8(N+1)}$ is a zero-one matrix, which contains one nonzero cell in each row and at most one nonzero cell in each column, under which configuration, the states are directly measured; $C_{n_r} = C_0\boldsymbol{\Phi}$, and $\boldsymbol{\Phi} = \boldsymbol{I}_2 \otimes \Phi$, and $\otimes$ is Kronecker product; G models fault effects on measurements; $v(t)$ is measurement noise. A state-space model can be formulated by letting $x(t) = [z^\top(t)\ \dot{z}^\top(t)]^\top \in \boldsymbol{R}^{2n_r}$, and

$$\begin{cases} \dot{x}(t) = Ax(t) + Ff(t) + Dw(t) \\ y(t) = Cx(t) + Gf(t) + v(t), \end{cases} \tag{3.5}$$

where

$$A = \begin{bmatrix} 0 & I \\ -K_{n_r} & -\omega G_{n_r} \end{bmatrix},\ F = \begin{bmatrix} 0 \\ F_{n_r} \end{bmatrix},\ D = \begin{bmatrix} 0 \\ D_{n_r} \end{bmatrix},\ C = C_{n_r},$$
$$w(t) \sim (0, Q^x),\ v(t) \sim (0, R).$$

When perfect information about $f(t)$ is known, *Kalman-Bucy filter* based state estimation can be constructed as [15]:

$$\dot{\hat{x}}(t) = A\hat{x}(t) + Ff(t) + K^x(t)\,[\,y(t) - C\hat{x}(t) - Gf(t)\,] \tag{3.6a}$$

$$K^x(t) = P^x(t)C^\top R^{-1} \tag{3.6b}$$

$$\dot{P}^x(t) = AP^x(t) + P^x(t)A^\top + DQ^xD^\top - P^x(t)C^\top R^{-1}CP^x(t), \tag{3.6c}$$

where $\hat{x}(t)$ is the state estimator, $P^x(t)$ is state estimation error covariance and $K^x(t)$ is Kalman gain. Note that when $f(t) \equiv 0$, all terms related to $f(t)$ will vanish; when $f(t)$ is a known signal, $f(t)$ acts as a known external excitation for the system, and the role of "fault" will turn into system input. Using either of the above two scenarios, the error covariance dynamics will not be affected.

Depending on how $K^x(t)$ is desired, either *Kalman-Bucy filter* or *steady-state Kalman filter* ($K^x(t) \equiv K^x(\infty)$) can be implemented. The state estimation error covariance dynamics $P^x(t)$ of *Kalman-Bucy filter* can be simulated following the Simulink structure outlined in [1]. Figure 3.1 presents the comparison between these two approaches when $f(t) \equiv 0$ and $f(t) \neq 0$ scenarios. For this simulation, the measurement model is adopted from [19], where 12 measurements are collected. As presented, *Kalman-Bucy filter* provides faster tracking results; when state estimation error covariance dynamics converges, both filters provide similar estimation results. More clearly, Figure 3.2 demonstrates the comparison of state estimation error covariance matrix trace of both filters. With zero initial condition guess on states and an initial guess of error covariance $P_0^x = 0.05\boldsymbol{I}$, *Kalman-Busy*

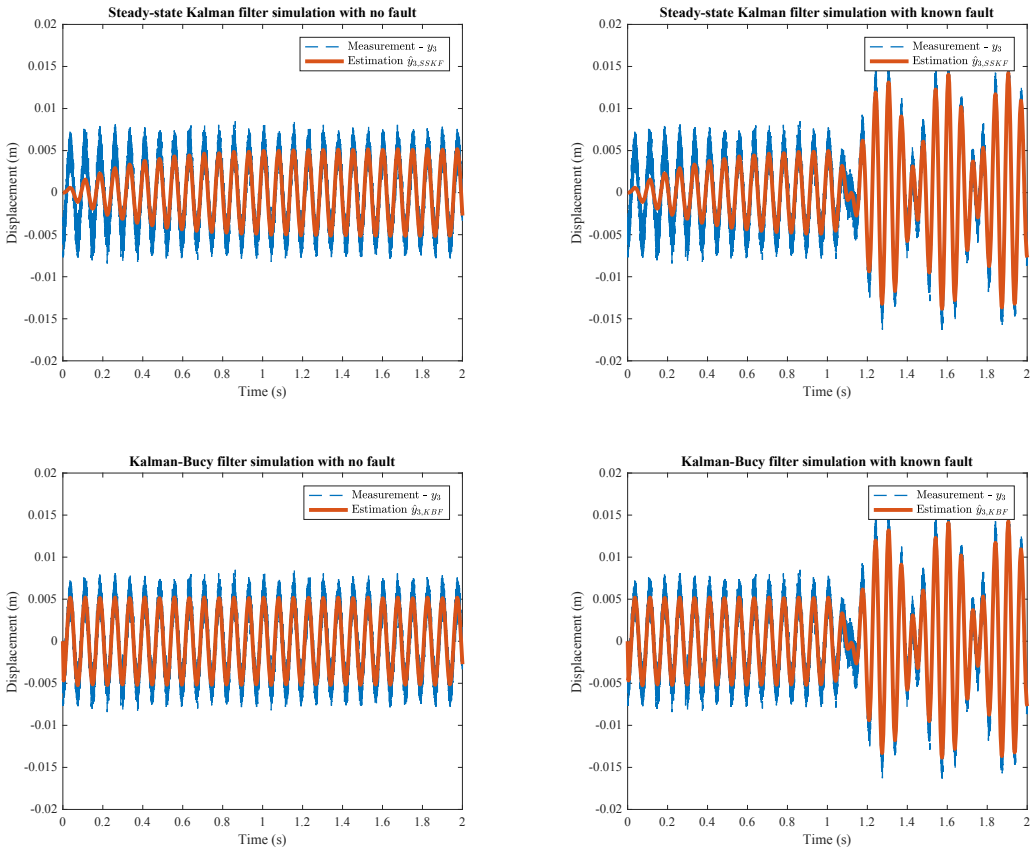

Figure 3.1: Output tracking of the center node x-direction displacement using two continuous Kalman filtering approaches for known fault cases.

filter firstly enhances correction on estimation to achieve faster tracking; eventually, both *Kalman-Bucy filter* and *steady-state Kalman filter* achieve the same steady-state of the trace value.

However, this simulation is performed based on reference measurement model applied in [19], which is chosen based on experience. It is hard to measure how good the estimation quality is given that 12 sensors are used. Questions such as whether fewer senors or different combinations of sensors will provide better results should be answered in a unified sensor selection algorithm.

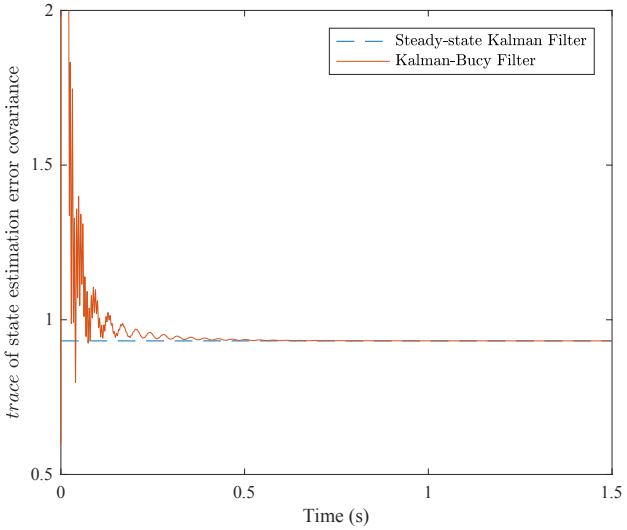

Figure 3.2: Trace of error covariance matrix comparison.

3.3 Optimal Sensor Selection Problem Formulation

3.3.1 Optimization Criteria

Recall the state estimation error covariance dynamics of *Kalman-Bucy filter*:

$$\dot{P}^x(t) = AP^x(t) + P^x(t)A^\top + DQ^xD^\top - P^x(t)C^\top R^{-1}CP^x(t). \tag{3.7}$$

The covariance dynamics is fixed and can be simulated offline once the system matrices and initial conditions are determined, namely, $P^x(t)$ is independent with actual measurements under conventional structure. Thus, formulating measurement model C_0, which is the only design variable in Equation 3.7 ($C = C_0 \cdot \mathbf{\Phi}$), that can improve certain performance measure of $P^x(t)$ is feasible. This is one of the major motivation of sensor selection topic [26].

The commonly used covariance metrics are as following [14]:

- $F_{1,t}(C_0) = \text{trace}(P^x(t))$: mean squared error;
- $F_{2,t}(C_0) = \max \text{eig}(P^x(t))$: worst-case error covariance;
- $F_{3,t}(C_0) = \log\det(P^x(t))$: volumn of confidence ellipsoid.

Even though it is analyzed in [14] that sensor selection problem is not, in general, submodular, an approximate optimal sensor selection solution can still be achieved to provide satisfactory performance. Analysis and simulation in Subsection 3.2.2 indicates that the

covariance dynamics can converge to steady-state in a very short amount of time, and thus, $F_{1,\infty}(C_0)$, $F_{2,\infty}(C_0)$ and $F_{3,\infty}(C_0)$ can be considered as the optimization criteria, and the easy computation of $P^x(\infty)$ is advantageous.

Remark 3.3.1 *It is necessary to point out that the sensor selection problem discussed in this context is different from sensor placement problem in mechanical and structural engineering. While sensor placement problem explicitly analyze where to place the sensors, sensor selection for optimal Kalman filtering emphasize the choices of system states to measure to ensure Kalman filtering performance. Therefore, sensor selection in this chapter aims at providing a guideline of preferred sensor location and type for practical instrumentation.*

3.3.2 Problem Formulation and Practical Specifications

Fundamental Assumption

The most fundamental assumption about state estimation problem is system observability. Recall the general measurement model defined in Equation (3.4), the generalized observability matrix for system in Equation (3.5) can be written as

$$W_{O,p} = \begin{bmatrix} C \\ CA \\ \vdots \\ CA^{p-1} \end{bmatrix} = \begin{bmatrix} C_0\mathbf{\Phi} \\ C_0\mathbf{\Phi}A \\ \vdots \\ C_0\mathbf{\Phi}A^{p-1} \end{bmatrix} = \begin{bmatrix} C_0\mathbf{\Phi} & & \\ & \ddots & \\ & & C_0\mathbf{\Phi} \end{bmatrix} \begin{bmatrix} A^0 \\ A \\ \vdots \\ A^{p-1} \end{bmatrix} = S_p(C_0\mathbf{\Phi}) \cdot Z_p(A),$$

where S and Z are two matrix functions. More specifically, $S(\cdot)$ is related to sensor selection and order reduction, and $Z(\cdot)$ is system property that insensitive to sensor selection. Since $\text{rank}(Z_p(A)) = 2n_r$, the full rank of $W_{O,p}$ is guaranteed when $S_p(C_0\mathbf{\Phi})$ is full column rank, namely, $m \geq 2n_r$. Thus, $|C| = 2n_r$ is the upper bound of sensor number for the optimal sensor selection problem, where $|\cdot|$ is cardinality measure.

Problem Formulation

There are different approaches to formulate sensor selection problems, and they are suitable for different estimation methods. Using system observability as a qualitative objective to optimally choose measurements is the dual problem of that proposed in [23], and it is more suitable for Luenberger observer based state estimation problem; the optimally selected minimum number of sensors ensure system observable, but estimation quality,

such as convergence speed and estimation smoothness, is not considered. Fisher information matrix (FIM) based sensor selection aims at minimizing the general inverse of FIM, which is the lower bound of covariance matrix of any unbiased estimator; while, in order to make FIM nonsingular, observability is required, and thus it is more suitable for trimming measurement model from a higher dimension.

For optimal Kalman filtering, covariance metrics based sensor selection can take advantage of the availability of state estimation error covariance dynamics, which quantifies estimation performance and provides insights of the estimation quality on stochastic systems. Thus, in general, the problem is formulated as finding the minimum number of sensors that guarantee covariance metrics ($F_{1,\infty}(C_0)$, $F_{2,\infty}(C_0)$ and $F_{3,\infty}(C_0)$) within certain threshold. The challenging aspect of this formulation is that a corresponding criterion threshold is required to be determined in advance, which can be very difficult to achieve in certain circumstances. It is worthwhile pointing out that even though there is no explicit requirement for observability in this formulation, but better metric values are achieved subject to system observability. In other word, when the metric value is optimized, system observability is achieved when metric value reaches certain level.

In this thesis, measurement model in [19] is used as reference; proposed algorithm aims at providing sensor selection solutions with better state estimation performance and fewer sensors required. Thus, an intuitive optimization problem is formulated as

$$\begin{aligned} &\min\ F_{i,\infty}(C_0) \\ &\text{s.t. } |C_0| \leq 2n_r. \end{aligned} \tag{3.8}$$

The optimization problem can be solved using the following approximation algorithm:

Approximation Algorithm - Optimal Sensor Selection

Input: $F_{i,\infty}$, C_0, V

Output: Approximate solution for C_0^*

while $|C_0| \leq 2n_r$

$a' \leftarrow \text{argmax}_{a \in V - C_0}\{F_{i,\infty}(C_0) - F_{i,\infty}(C_0 \cup \{a\})\}$

$C_0 \leftarrow C_0 \cup a'$

end while

where V is the entire sensor or measurement set, amd a' is the best selection under current iteration. In order to ease the computation, $F_{i,\infty}(C)$ is used for the simulation. Moreover,

the sensor number upper bound specification significantly reduces the number of iterations of approximation algorithm, since $2n_r \ll 4(N+1)$.

Remark 3.3.2 *In practical applications, input C_0 is a set of pre-selected measurements, which are strongly preferred due to instrumentation reasons. In this case, the initial feasible sensor set should be defined as $\bar{V} = V - C_0$. Meanwhile, based on real setup, locations where sensors are not possible to be mounted can be excluded from V, such that the algorithm will not output sensor sections from these locations.*

3.4 Simulation Results and Conclusion

3.4.1 Comparison of Different Covariance Metrics

Simulation of selection through 1 to $2n_r$ sensors are compared with both reference measurement model and full information case, where all $2(N+1)$ states are measured, and the results are shown in Figure 3.3. The following observations can be concluded:

- As the number of measurements increase, the covariance metric values decrease and approach full information covariance metric.
- As the number of measurements increase, the metric value decrement becomes smaller. This is the supermodularity property of the covariance metrics.

These two observations essentially indicate that adding more sensors will improve estimation performance, but once the number of measurements is big enough, it is not economical to adding more sensors due to the estimation improvement will not match the linearly increasing cost of extra sensors.

Another observation that can be drawn from all three metrics simulation is that, in order to achieve the same estimation quality as the reference measurement model, the sensor selection algorithm outputs much smaller number. This observation proves the effectiveness of applying the selection algorithm.

3.4.2 Sensor Selection Subject to Sensor Type Limitations

Simulation in Subsection 3.4.1 allows measurements to be collected from all state variables. Practically, this assumption is difficult to be achieved due to either hardware limitation or system physical structures. Compared to vibration displacement and velocity measurements, angular displacement and velocity measurements are more challenging to

collect. Therefore, certain limitations should be imposed in the measurement model before performing the algorithm.

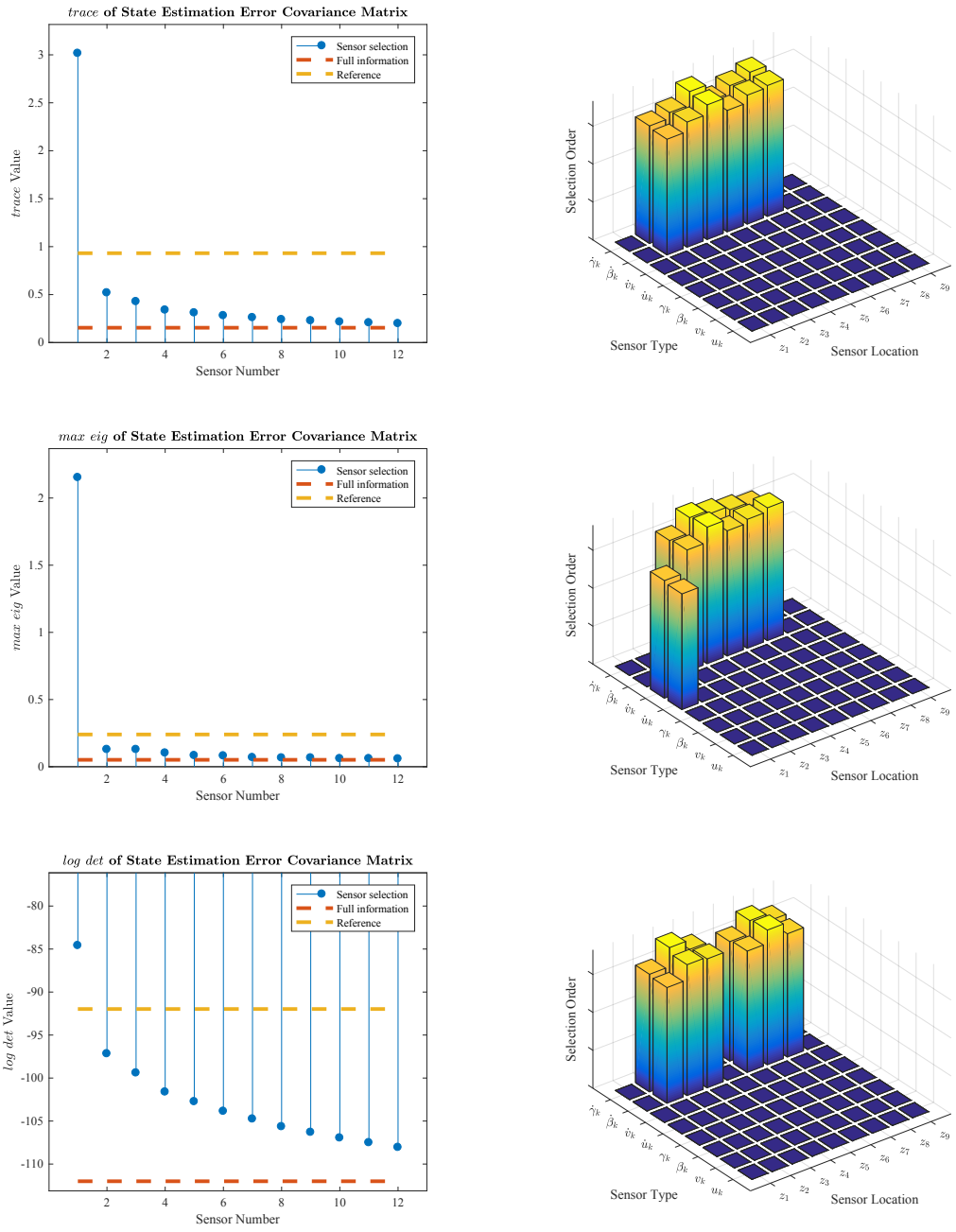

Figure 3.3: Sensor selection among all state variables and comparison of metric values between approximate algorithm, reference model and full information cases.

Selection Among Vibration Displacement or Velocity Measurements Only

In order to compare the effectiveness of displacement and velocity measurement on state estimation, Figure 3.4 illustrates some important observations: (i) the type of measurements makes significant difference in optimal sensor selection, and (ii) especially in the system model presented in this thesis, velocity measurements are far more effective in lowering covariance metric values than displacement measurements. Comparing to Figure 3.3, the angular velocity measurements are the most effective among all the state variables.

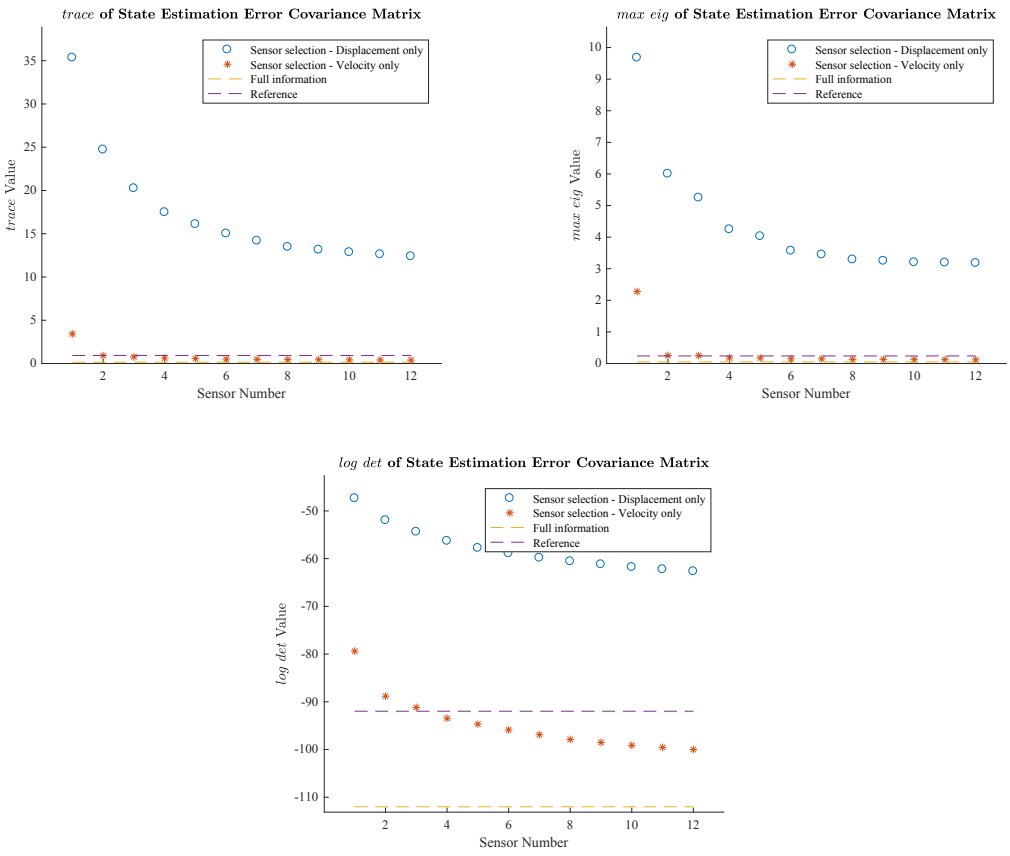

Figure 3.4: Sensor selection comparison between displacement and velocity measurements.

Selection Result Using Complex Sensors

Thanks to the development of sensor technology, large amount of vibration sensors can manage to measure both displacement and velocity, or even acceleration at the same time with one equipment. In this case, sensor selection problem can be further reduced to node/location selection. Figure 3.5 demonstrates the simulation result using these complex sensors.

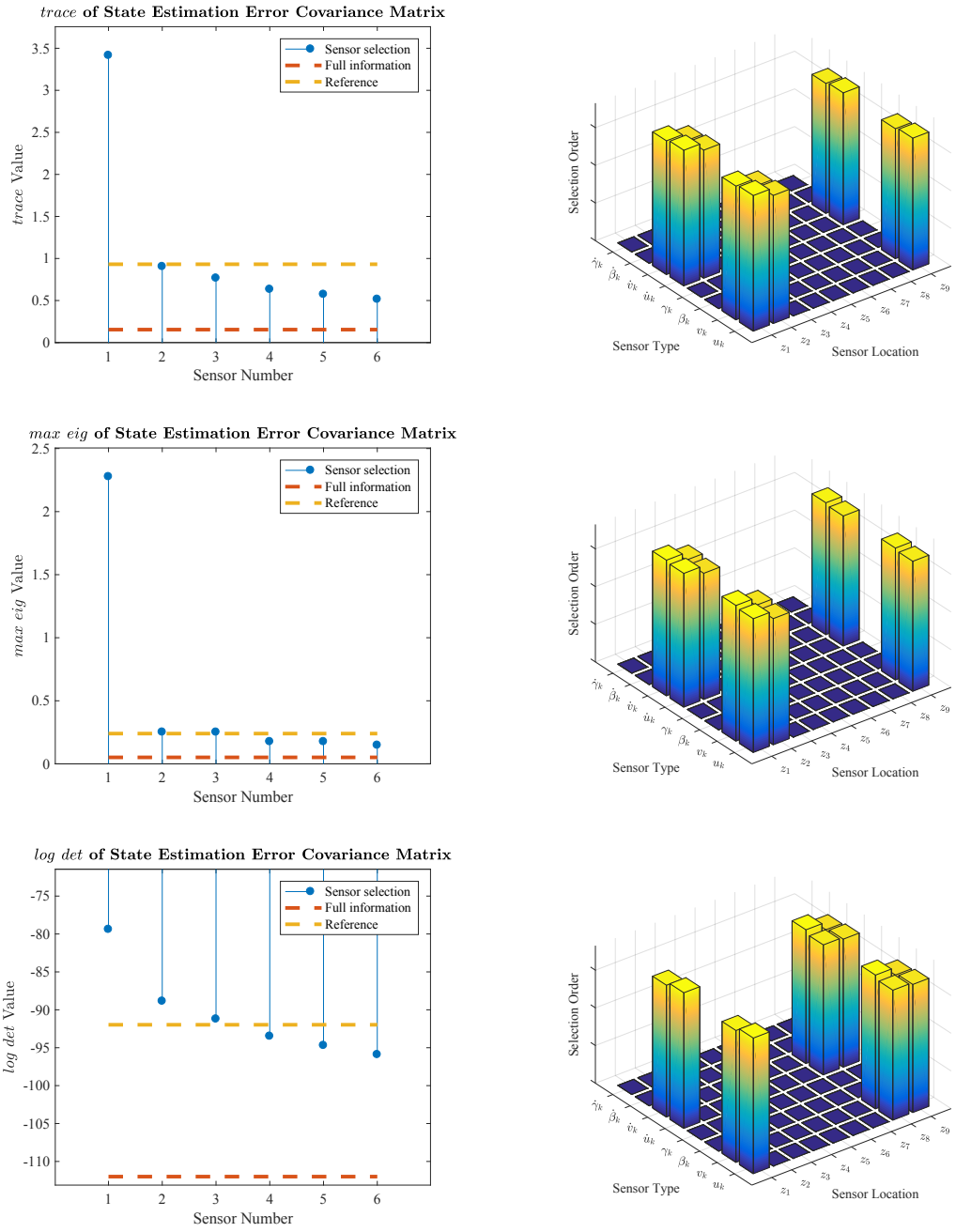

Figure 3.5: Sensor selection using complex vibration sensors.

3.4.3 State Estimation Performance

Figure 3.6 illustrates the comparison of error covariance trace between optimally selected measurement model with 10 measurements and reference model with 12 measurements . As expected, sensor selection provide a measurement model with smaller trace.

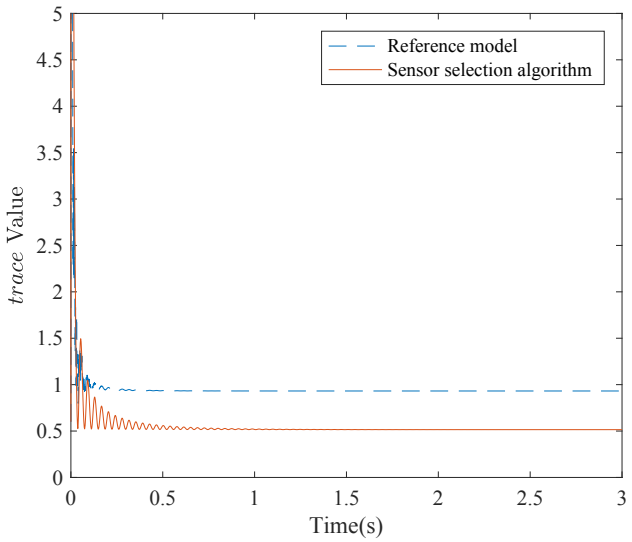

Figure 3.6: Comparison of state estimation error covariance trace between reference model and sensor selection result.

Assume $\hat{f}(t)$ is the estimate of $f(t)$, and output tracking error expectation can be written as $\boldsymbol{E}[e_y(t)] = \boldsymbol{E}[y(t) - \hat{y}(t)] = \boldsymbol{E}\left[C(x(t) - \hat{x}(t)) + G(f(t) - \hat{f}(t))\right] + \boldsymbol{E}[v(t)]$, and its covariance as

$$
\begin{aligned}
&\boldsymbol{E}\left[e_y(t)e_y(t)^\top\right] \\
&\quad = \boldsymbol{E}\left[(y(t) - \hat{y}(t))(y(t) - \hat{y}(t))^\top\right] \\
&\quad = \boldsymbol{E}\left[C(x(t) - \hat{x}(t))(x(t) - \hat{x}(t))^\top C^\top + G(f(t) - \hat{f}(t))(f(t) - \hat{f}(t))^\top G^\top\right] + \boldsymbol{E}\left[v(t)v^\top(t)\right].
\end{aligned}
$$

Although sensor selection has rendered state estimation error covariance trace smaller than reference model, the output tracking error covariance trace is not as advantageous. Figure 3.7 demonstrates output tracking error covariance trace when $f(t)$ is known, in which case, $f(t)$ is deterministic, namely, $\hat{f}(t) \equiv f(t)$. This can be explained by the fact that optimal sensor selection has chosen measurements close to bearings, which, according to the system first mode shape, have very small magnitude and are closely affected by modeling error. Thus, these measurements tend to be noisier than those from central part of the rotor. When fault is known, both output tracking is satisfactory because the trace values are below or close by the threshold, which is calculated as

$$
\begin{aligned}
\text{threshold} &= \mathrm{Tr}\{\boldsymbol{E}\left[C(x(t) - \hat{x}(t))(x(t) - \hat{x}(t))^\top C^\top\right] + \boldsymbol{E}\left[v(t)v^\top(t)\right]\} \\
&= \mathrm{Tr}\{CP(t)C^\top + R\}.
\end{aligned}
$$

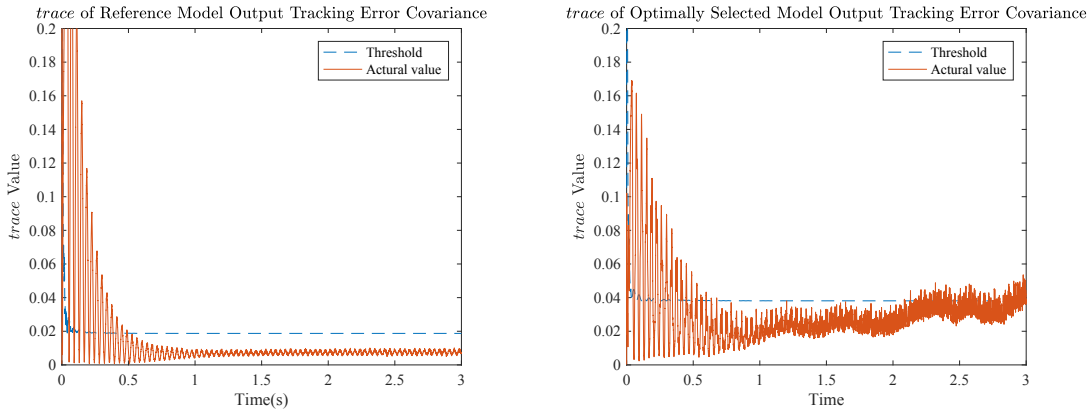

Figure 3.7: Comparison of innovation covariance trace with corresponding threshold between reference model and sensor selection result when no fault exists.

While $f(t)$ is stochastic or unknown, the output tracking error covariance trace is presented in Figure 3.8. As is shown, both model can sensitively detect the modeled fault dynamics. The optimal sensor selection model is less sensitive comparing to the reference model due to its signal-to-noise ratio is lower.

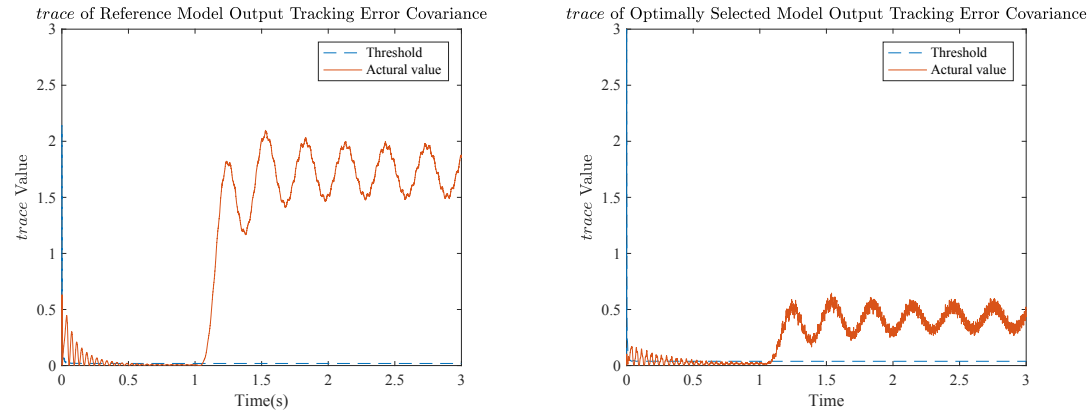

Figure 3.8: Comparison of innovation covariance trace with corresponding threshold between reference model and sensor selection result when fault exists.

3.4.4 Conclusion

The optimization-based sensor selection method studied in this chapter presents a framework to design a measurement model to achieve designed state estimation performance. An approximation algorithm is outlined for implementation and practical limitations or constraints can be added to calculate more appropriate sensor solution. Through various simulations, the byproduct of the sensor selection algorithm is more insightful observations of the the model and measurements, which is very helpful for practice. However, the fact that the false alarms have occurred when applying optimal sensor selection also indicates that for real applications, more system property related constraints should be added to provide more accurate filtering solution.

As mentioned in state estimation performance, when ummodeled fault occurs, conventional Kalman filtering will not be able to provide accurate estimation results due to the dramatic dynamics changes in output tracking errors. In order to maintain the estimation performance, the potential faults should also be modeled.

Chapter 4

Simultaneous State and Fault Estimation via Kalman Filtering

4.1 Introduction

In Chapter 3, optimal Kalman filtering based state estimation and sensor selection problems have been investigated assuming fault dynamic $f(t)$ is perfectly known, in which case, fault signal acts as system external input. Generally, information of $f(t)$ is incomplete or unknown, and the original filtering structure may fail to provide accurate state estimation due to the abnormal changes in system structure resulted from unmodeled fault dynamics [12]. More specifically, the optimality of Kalman filtering designed based on fault-free system model generally degrades when fault occurs. Therefore, modeling and estimation of the fault dynamics are required for maintaining state estimation performance.

One of the most intuitive strategies for simultaneous state and fault estimation is *augmented state Kalman filter* (ASKF), where fault states are augmented with the fault-free system states such that a higher order Kalman filtering structure can be implemented, and optimal estimation is achieved with more intensive computation load. *Optimal two-stage Kalman filter* (OTSKF) proposed in [11] presents an equivalent form of ASKF with two decoupled lower order filters. Even though the computation efficiency is not necessarily superior compared to ASKF for all types of system matrices structures [20], the idea of feeding innovation signal driven compensation to fault-free filtering structure is advantageous for implementation of Kalman filtering based fault estimation.

This chapter studies simultaneous state and fault estimation for simple rotor-bearing systems via Kalman filtering. Thanks to the innovation of OTSKF, the already established

state estimation framework from previous chapters will be inherited; in addition, a fault filter is then designed to generate compensation based on innovation sequence from the fault-free filtering. Further, an adaptive algorithm is utilized to achieve automatic adjustment to OTSKF in order to handle Kalman filtering performance degrading or diverging issues caused by sudden dynamic changes.

4.2 Preliminary

4.2.1 Discretized System Representation

Thanks to the simple form of *Kalman-Bucy filter* described in Equation (3.6) for analysis, previous study on rotor-bearing system state estimation and sensor selection are conducted in continuous time case. In reality, continuous measurements are either impossible or too expensive to collect. Thus, a discretized system representation is necessary for implementation purpose. Apply Euler's approximation on system Equation (3.5), and the following discrete state-space model can be obtained:

$$\begin{cases} x_{k+1} = A_k x_k + F_k f_k + D_k w_k \\ y_k = C_k x_k + G_k f_k + v_k, \end{cases} \tag{4.1}$$

where A_k, C_k and D_k are discretized system matrices under fixed sampling period T, and T is assumed to be small enough to ensure numerical precision. *Kalman filter* can be then formulated for the discretized system as:

$$\hat{x}_{k|k-1} = A_{k-1}\hat{x}_{k-1|k-1} + F_{k-1}f_{k-1} \tag{4.2a}$$

$$P^x_{k|k-1} = A_{k-1}P^x_{k-1|k-1}A^\top_{k-1} + Q^x_{k-1} \tag{4.2b}$$

$$K^x_k = P^x_{k|k-1}C^\top_k (C_k P^x_{k|k-1} C^\top_k + R_k)^{-1} \tag{4.2c}$$

$$P^x_{k|k} = (I - K^x_k C_k) P^x_{k|k-1} \tag{4.2d}$$

$$\hat{x}_{k|k} = \hat{x}_{k|k-1} + K^x_k (y_k - C_k \hat{x}_{k|k-1} - G_k f_k), \tag{4.2e}$$

where $Q^x_k = D_k Q_k D^\top_k$. In this thesis, the spectral density matrices for disturbance, Q^x, and measurement noise, R, are considered constant, thus, $Q^x_k = TQ^x$ and $R_k = R/T$ [18]. It is worth pointing out that, even though *Kalman filter* is not a simple sampling of *Kalman-Bucy filter*, the following relations still hold:

$$\hat{x}(kT) = \hat{x}_{k|k}, \;\; K^x(kT) = \frac{1}{T}K^x_k, \;\; P^x(kT) = P^x_{k|k-1}.$$

Thus, sensor selection studied in Chapter 3, which is based on *Kalman-Bucy filter* state estimation error covariance dynamics described in Equation (3.7), is equivalent to sensor selection problem based on *a priori* error covariance matrix in *Kalman filter*. Therefore, sensor selection algorithm studied in Chapter 3 can be directly applied in discrete-time case when *a priori* error covariance matrix is applied to measure estimation performance.

4.2.2 Augmented State System Representation

According to Equation (2.16), imbalance fault can be modeled as an external imbalance force input in terms of q_ε and $\dot{q}_\varepsilon$. Let $f_k = [q_\varepsilon^\top(t)\ \dot{q}_\varepsilon^\top(t)]_{t=kT}^\top$, and the system of interest can be then reformulated by introducing fault dynamics as:

$$\begin{cases} x_{k+1} = A_k x_k + F_k f_k + D_k w_k \\ f_{k+1} = H_k f_k + E_k d_k \\ y_k = C_k x_k + G_k f_k + v_k, \end{cases} \tag{4.3}$$

where H_k is fault dynamic matrix and E_k is fault modeling error matrix. Correspondingly, an augmented state space model can be formed as

$$\begin{cases} \bar{X}_{k+1} = \bar{A}_k \bar{X}_k + \bar{W}_k \\ y_k = \bar{C}_k X_k + v_k, \end{cases} \tag{4.4}$$

where

$$\bar{X}_k = \begin{bmatrix} x_k \\ f_k \end{bmatrix},\ \bar{A}_k = \begin{bmatrix} A_k & F_k \\ 0 & H_k \end{bmatrix},\ \bar{W}_k = \begin{bmatrix} D_k w_k \\ E_k d_k \end{bmatrix},\ \bar{C}_k = \begin{bmatrix} C_k & G_k \end{bmatrix}.$$

Assume fault modeling error d_k is uncorrelated with w_k, and thus,

$$\boldsymbol{E}[\bar{W}_k \bar{W}_k^\top] = \begin{bmatrix} Q_k^x & 0 \\ 0 & Q_k^f \end{bmatrix}. \tag{4.5}$$

Therefore, *augmented state Kalman filter* (ASKF) can be designed according to conventional *Kalman filter* structure described in Equation (4.2), such that simultaneous estimation of states and imbalance faults can be achieved.

Remark 4.2.1 *In order to achieve optimal estimation, fault dynamic matrices H_k and E_k are assumed to be accurate in this thesis. However, in real applications, identification techniques may be required to improve accuracy of these matrices.*

Remark 4.2.2 *The assumption described in Equation (4.4) is very ideal. In general, imbalance fault modeling error d_k will increase disturbance or uncertainty of dynamic of x_k, and the correlation of d_k and w_k is expected. While the idealized uncorrelation assumption is often used in application of two-stage Kalman filter, in this thesis, it is used to simplify analysis.*

4.3 Adaptive Two-Stage Kalman Filter for Imbalance Estimation

4.3.1 Limitation of Using Augmented-State Kalman Filter for Imbalance Fault Estimation

Given discrete state-space model described in Equation (4.4), ASKF is optimal in the sense of minimum mean squared error (MSE):

$$\hat{\bar{X}}_{k|k-1} = \bar{A}_{k-1}\hat{\bar{X}}_{k-1|k-1} \tag{4.6a}$$

$$\bar{P}_{k|k-1} = \bar{A}_{k-1}\bar{P}_{k-1|k-1}\bar{A}_{k-1}^{\top} + \bar{Q}_{k-1} \tag{4.6b}$$

$$\bar{K}_k = \bar{P}_{k|k-1}\bar{C}_k^{\top}(\bar{C}_k\bar{P}_{k|k-1}\bar{C}_k^{\top} + R_k)^{-1} \tag{4.6c}$$

$$\bar{P}_{k|k} = (I - \bar{K}_k\bar{C}_k)\bar{P}_{k|k-1} \tag{4.6d}$$

$$\hat{\bar{X}}_{k|k} = \hat{\bar{X}}_{k|k-1} + \bar{K}_k(y_k - \bar{C}_k\hat{\bar{X}}_{k|k-1}), \tag{4.6e}$$

where "$\bar{\cdot}$" indicates augmented vectors or matrices, and "$\hat{\cdot}$" represents estimated vectors, and the combination "$\hat{\bar{\cdot}}$" indicates the specific estimate is obtained based on the augmented state system model. More specifically,

$$\hat{\bar{X}}_{(\cdot)} = \begin{bmatrix} \hat{\bar{x}}_{(\cdot)} \\ \hat{\bar{f}}_{(\cdot)} \end{bmatrix}, \quad \bar{P}_{(\cdot)} = \begin{bmatrix} \bar{P}^{x}_{(\cdot)} & \bar{P}^{xf}_{(\cdot)} \\ \bar{P}^{fx}_{(\cdot)} & \bar{P}^{f}_{(\cdot)} \end{bmatrix}, \quad \bar{K}_{(\cdot)} = \begin{bmatrix} \bar{K}^{x}_{(\cdot)} \\ \bar{K}^{f}_{(\cdot)} \end{bmatrix},$$

Besides the intensive computation complexity of higher dimensional matrix inverse associated with ASKF, there are some other practical disadvantages:

- For imbalance faults commonly existed in rotor-bearing systems, they can be located at multiple locations. Since the number of imbalance locations may not be known, the fault model is subject to modification or switching for different scenarios. This issue will result in a re-design of the entire ASKF due to the augmentation. However,

it is more advantageous for implementation if the main structure of system state estimation can be retained but only fault estimation structure needs to be re-designed for different fault scenarios.

- On the other hand, for real structural systems that faults may not occur at the early stage of operation, ASKF is not efficient since lower order *Kalman filter* designed based on fault-free system representation can perform well enough for state estimation. Additionally in this case, when fault eventually occurs after long period of time of operation, the degradation of Kalman filtering may lead to inaccurate or diverging estimate of both the states and fault [28].

4.3.2 Optimal Two-Stage Kalman Filter

The core idea behind *optimal two-stage Kalman filter* (OTSKF) is to construct two lower order filters ($\hat{x}_{(\cdot)}$ and $\hat{f}_{(\cdot)}$ with $P^x_{(\cdot)}$ and $P^f_{(\cdot)}$) that can be linearly combined to achieve an equivalence of ASKF described in Equation (4.6), so that the optimality is automatically guaranteed. According to [11], the OTSKF can be described as following forms:

$$\hat{\bar{x}}_{k|k-1} = \hat{x}_{k|k-1} + U_k \hat{f}_{k|k-1} \tag{4.7a}$$

$$\bar{P}^x_{k|k-1} = P^x_{k|k-1} + U_k P^f_{k|k-1} U_k^\top \tag{4.7b}$$

$$\hat{\bar{x}}_{k|k} = \hat{x}_{k|k} + V_k \hat{f}_{k|k} \tag{4.7c}$$

$$\bar{P}^x_{k|k} = P^x_{k|k} + V_k P^f_{k|k} V_k^\top, \tag{4.7d}$$

where

Bias-Free Filter

$$\hat{x}_{k|k-1} = A_{k-1}\hat{x}_{k-1|k-1} + (\bar{U}_k - U_k) H_{k-1} \hat{f}_{k-1|k-1} \tag{4.8a}$$

$$P^x_{k|k-1} = A_{k-1} P^x_{k-1|k-1} A_{k-1}^\top + Q^x_{k-1} + U_k (\bar{U}_k Q^f_{k-1})^\top \tag{4.8b}$$

$$K^x_k = P^x_{k|k-1} C_k^\top (C_k P^x_{k|k-1} C_k^\top + R_k)^{-1} \tag{4.8c}$$

$$P^x_{k|k} = (I - K^x_k C_k) P^x_{k|k-1} \tag{4.8d}$$

$$\hat{x}_{k|k} = \hat{x}_{k|k-1} + K^x_k (y_k - C_k \hat{x}_{k|k-1}); \tag{4.8e}$$

Bias Filter

$$\hat{f}_{k|k-1} = H_{k-1}\hat{f}_{k-1|k-1} \tag{4.9a}$$

$$P^f_{k|k-1} = H_{k-1}P^f_{k-1|k-1}H^\top_{k-1} + Q^f_{k-1} \tag{4.9b}$$

$$K^f_k = P^f_{k|k-1}S^\top_k(C_kP^x_{k|k-1}C^\top_k + R_k + S_kP^f_{k|k-1}S^\top_k)^{-1} \tag{4.9c}$$

$$P^f_{k|k} = (I - K^f_kS_k)P^f_{k|k-1} \tag{4.9d}$$

$$\hat{f}_{k|k} = \hat{f}_{k|k-1} + K^f_k(y_k - C_k\hat{x}_{k|k-1} - S_k\hat{f}_{k|k-1}); \tag{4.9e}$$

Coupling Equations

$$\bar{U}_k = (A_{k-1}V_{k-1} + F_{k-1})H^{-1}_{k-1} \tag{4.10}$$

$$U_k = \bar{U}_k[I - Q^f_{k-1}(P^f_{k|k-1})^{-1}] \tag{4.11}$$

$$S_k = C_kU_k + G_k \tag{4.12}$$

$$V_k = U_k - K^x_kS_k. \tag{4.13}$$

The fault estimates of ASKF have much simpler relations with those of OTSKF as

$$\hat{\bar{f}}_{k|k-1} = \hat{f}_{k|k-1},\ \ \hat{\bar{P}}^f_{k|k-1} = \hat{P}^f_{k|k-1},\ \ \hat{\bar{f}}_{k|k} = \hat{f}_{k|k},\ \ \hat{\bar{P}}^f_{k|k} = \hat{P}^f_{k|k}. \tag{4.14}$$

The detailed derivation is provided in the appendix of [11].

Remark 4.3.1 *Due to assumption imposed on fault modeling error and system disturbance described in Equation (4.5), the algebraic constraint required to ensure the equivalence between OTSKF and ASKF described in [11] is significantly simplified to*

$$Q^x_k + U_{k+1}(\bar{U}_{k+1}Q^f_k)^\top \geq 0.$$

It is worth pointing out that this constrain is guaranteed under Equation (4.5), since Q^x_k and Q^f_k are symmetric and positive definite, and

$$Q^x_k + U_{k+1}(\bar{U}_{k+1}Q^f_k)^\top = Q^x_k + \bar{U}_{k+1}[Q^f_k - Q^f_{k-1}(P^f_{k|k-1})^{-1}Q^f_k]\bar{U}^\top_{k+1},$$

which indicates that $Q^x_k + U_{k+1}(\bar{U}_{k+1}Q^f_k)^\top$ is symmetric, and thus positive semidefinite. Therefore, the constraint is guaranteed.

Note that when f_k is constant or perfectly known, $Q_k^f = 0$, $U_k = \bar{U}_k$, $\hat{f}_{k|k} = \hat{f}_{k|k-1} = H_{k-1}\hat{f}_{k-1|k-1} = H_{k-1}f_{k-1} = f_k$, and thus,

$$\begin{aligned}
\hat{\hat{x}}_{k|k-1} &= A_{k-1}\hat{x}_{k-1|k-1} + (A_{k-1}V_{k-1} + F_{k-1})H_{k-1}^{-1} \cdot H_{k-1}f_{k-1} \\
&= A_{k-1}(\hat{x}_{k-1|k-1} + V_{k-1}f_{k-1}) + F_{k-1}f_{k-1} \\
&= A_{k-1}\hat{\hat{x}}_{k-1|k-1} + F_{k-1}f_{k-1} \\
\hat{\hat{x}}_{k|k} &= \hat{x}_{k|k-1} + K_k^x(y_k - C_k\hat{x}_{k|k-1}) + [(A_{k-1}V_{k-1} + F_{k-1})H_{k-1}^{-1} - K_k^x(C_kU_k + G_k)] \cdot H_{k-1}f_{k-1} \\
&= \hat{\hat{x}}_{k|k-1} + K_k^x(y_k - C_k\hat{\hat{x}}_{k|k-1} - G_kf_k),
\end{aligned}$$

which is exactly the conventional *Kalman filter* described in Equation (4.2). In other word, OTSKF is reduced to bias-free filter when f_k is perfectly known; bias-free filter in this case is exactly the same as Equation (4.2), filter designed based on fault-free model. The practical interpretation of this observation is that when fault has not occurred, *Kalman filter* designed for normal system is optimal; if fast fault detection can be established, bias filter can then be triggered to start estimating the faults, in which case, optimal estimate is still achieved. This strategy has great practical value in machineries that generally starts with normal operation.

4.3.3 Adaptive Fading Factor Design

Kalman filtering provides optimal estimate for linear Gaussian systems, and one of the important properties is that the innovation is a white noise when optimal gain is used. More specifically, for ASKF in Equation (4.6), the innovation is defined as

$$\bar{\eta}_k = y_k - \bar{C}_k\hat{\bar{X}}_{k|k-1}, \tag{4.15}$$

and its covariance and auto-covariance can be calculated as the following forms:

$$\begin{aligned}
\bar{\boldsymbol{C}}_{0,k} &= \boldsymbol{E}[\bar{\eta}_k\bar{\eta}_k^\top] = \bar{C}_k\bar{P}_{k|k-1}\bar{C}_k^\top + R_k, \\
\bar{\boldsymbol{C}}_{j,k} &= \boldsymbol{E}[\bar{\eta}_{k+j}\bar{\eta}_k^\top] = \boldsymbol{\Phi}_{k+j,\cdots,k+1} \cdot (\bar{P}_{k|k-1}\bar{C}_k^\top - \bar{K}_k\bar{\boldsymbol{C}}_{0,k}),
\end{aligned}$$

where $\boldsymbol{\Phi}_{k+j,\cdots,k+1}$ is a matrix that relates to future system matrices [28]. Denote

$$\boldsymbol{S}_k = \bar{P}_{k|k-1}\bar{C}_k^\top - \bar{K}_k\bar{\boldsymbol{C}}_{0,k}. \tag{4.16}$$

When optimal gain $\bar{K}_k$ is utilized for filtering, $\bar{\boldsymbol{C}}_{j,k}$ equals zero due to

$$\boldsymbol{S}_k = \bar{P}_{k|k-1}\bar{C}_k^\top - \bar{P}_{k|k-1}\bar{C}_k^\top(\bar{C}_k\bar{P}_{k|k-1}\bar{C}_k^\top + R_k)^{-1}(\bar{C}_k\bar{P}_{k|k-1}\bar{C}_k^\top + R_k) = 0.$$

However, this equality may fail when abnormal dynamics occur in the system described by Equation (4.4) whether the abnormal dynamics are modeled or unmodeled, and the real innovation covariance is altered approximately to

$$\tilde{\bar{\boldsymbol{C}}}_{0,k} = \frac{1}{n_w - 1} \sum_{i=k-n_w+1}^{k} \bar{\eta}_i \bar{\eta}_i^{\top}, \tag{4.17}$$

where n_w is the window size. One classical adaptive fading structure to maintain the equality in Equation (4.16) can be written as following:

$$\bar{\lambda}_k \bar{P}_{k|k-1} \bar{C}_k^{\top} - \bar{K}_k \tilde{\bar{\boldsymbol{C}}}_{0,k} = 0, \tag{4.18}$$

where $\bar{\lambda}_k$ is the adapting factor. Therefore, the optimality of *Kalman filter* with respect to Equation (4.16) is always achieved. It should be clarified that the adaptive factor $\bar{\lambda}_k$ aims at updating *Kalman filter* structure with innovation covariance information, which reflects sudden changes rather than unmodeled error dynamics in system dynamics; those unmodeled errors may further introduce bias into innovation sequence, in which case, Equation (4.18) is not sufficient enough to ensure state estimation performance.

Remark 4.3.2 *One of the most important applications of ASKF is parameter identification, where the value of those parameters are typically non-zero when measurements start to be collected for estimation. Fault estimation falls into a different scenario where f_k may not occur as soon as operation starts. When f_k occurs, since Kalman filter has already heavily adapted to the non-fault data, it may fail to capture the sudden changes and estimation may degrade or diverge, even when f_k is perfectly modeled.*

The following analysis aims at deriving the equivalent form of $\bar{\lambda}_k$ in Equation (4.18) using *two-stage Kalman filter* structure. In order to achieve this goal, the equivalence of ASKF innovation $\bar{\eta}_k$ and criterion in Equation (4.18)in OTSKF should be derived.

Innovation for Adaptive Fading Factor Calculation

In OTSKF, there are two innovation sequences for *bias-free filter* and *bias filter*, respectively, and are defined as

$$\eta_k^x = y_k - C_k \hat{x}_{k|k-1} \tag{4.19}$$

$$\eta_k^f = y_k - C_k \hat{x}_{k|k-1} - S_k \hat{f}_{k|k-1} = \eta_k^x - S_k \hat{f}_{k|k-1}. \tag{4.20}$$

Unless $\hat{f}_{k|k-1} \equiv 0$, at least one of these two innovation sequences are not zero-mean. Further expending the Equation (4.19), we can obtain the following result:

$$\begin{aligned}
\eta_k^x =& y_k - C_k\hat{x}_{k|k-1} \\
=& C_k(A_{k-1}x_{k-1} + F_{k-1}f_{k-1} + D_{k-1}w_{k-1}) + G_k(H_{k-1}f_{k-1} + E_{k-1}d_{k-1}) + v_k \\
& - C_k(A_{k-1}\hat{x}_{k-1|k-1} + (\bar{U}_k - U_k)H_{k-1}\hat{f}_{k-1|k-1}) \\
=& C_kA_{k-1}(x_{k-1} - \hat{x}_{k-1|k-1} - V_{k-1}\hat{f}_{k-1|k-1}) + C_kD_{k-1}w_{k-1} + v_k + G_kE_{k-1}d_{k-1} \\
& + (C_kF_{k-1} + G_kH_{k-1})f_{k-1} - C_k(\bar{U}_k - U_k - A_{k-1}V_{k-1}H_{k-1}^{-1})H_{k-1}\hat{f}_{k-1|k-1} \\
=& C_kA_{k-1}(x_{k-1} - \hat{\hat{x}}_{k-1|k-1}) + C_kD_{k-1}w_{k-1} + v_k + G_kE_{k-1}d_{k-1} \\
& + (C_kF_{k-1} + G_kH_{k-1})f_{k-1} - C_k(F_{k-1}H_{k-1}^{-1} - U_k)H_{k-1}\hat{f}_{k-1|k-1} \\
=& C_kA_{k-1}(x_{k-1} - \hat{\hat{x}}_{k-1|k-1}) + C_kD_{k-1}w_{k-1} + v_k + G_kE_{k-1}d_{k-1} \\
& + (C_kF_{k-1} + G_kH_{k-1})f_{k-1} - C_kF_{k-1}\hat{f}_{k-1|k-1} + (S_k - G_k)H_{k-1}\hat{f}_{k-1|k-1} \\
=& C_kA_{k-1}(x_{k-1} - \hat{\hat{x}}_{k-1|k-1}) + C_kD_{k-1}w_{k-1} + v_k + G_kE_{k-1}d_{k-1} \\
& + (C_kF_{k-1} + G_kH_{k-1})(f_{k-1} - \hat{\hat{f}}_{k-1|k-1}) + S_kH_{k-1}\hat{f}_{k-1|k-1}.
\end{aligned}$$

Due to $\hat{\hat{x}}_{k-1|k-1}$ and $\hat{\hat{f}}_{k-1|k-1}$ are the unbiased estimates of x_{k-1} and f_{k-1} from ASKF, thus $\boldsymbol{E}(x_{k-1} - \hat{\hat{x}}_{k-1|k-1}) = \mathbf{0}$ and $\boldsymbol{E}(f_{k-1} - \hat{\hat{f}}_{k-1|k-1}) = \mathbf{0}$, and thus

$$\boldsymbol{E}(\eta_k^x) = S_kH_{k-1}\boldsymbol{E}(\hat{\hat{f}}_{k-1|k-1}) = S_k\boldsymbol{E}(\hat{f}_{k|k-1}) \tag{4.21}$$

$$\boldsymbol{E}(\eta_k^f) = \boldsymbol{E}(\eta_k^x - S_k\hat{f}_{k|k-1}) = 0. \tag{4.22}$$

Equation (4.21) confirms that when f_k occurs, bias exist in innovation sequence, and thus, the innovation of *bias-free filter* is not white noise anymore. Moreover, since

$$\begin{aligned}
\eta_k^f =& y_k - C_k\hat{x}_{k|k-1} - S_k\hat{f}_{k|k-1} \\
=& y_k - C_k(\hat{\hat{x}}_{k|k-1} - U_k\hat{f}_{k|k-1}) - (C_kU_k + G_k)\hat{f}_{k|k-1} \\
=& y_k - C_k\hat{\hat{x}}_{k|k-1} - G_k\hat{\hat{f}}_{k|k-1} \\
=& \bar{\eta}_k,
\end{aligned}$$

and

$$\begin{aligned}
\boldsymbol{C}_{0,k}^{f} &= \boldsymbol{E}[\eta_k^f(\eta_k^f)^\top] \\
&= C_k P_{k|k-1}^{x} C_k^\top + R_k + S_k P_{k|k-1}^{f} S_k^\top \\
&= C_k P_{k|k-1}^{x} C_k^\top + R_k + (C_k U_k + G_k) P_{k|k-1}^{f} (C_k U_k + G_k)^\top \\
&= C_k P_{k|k-1}^{x} C_k^\top + G_k P_{k|k-1}^{f} U^\top C_k^\top + C_k U_k P_{k|k-1}^{f} G_k^\top + G_k P_{k|k-1}^{f} G_k^\top + R_k \\
&= \bar{C}_k \bar{P}_{k|k-1} \bar{C}_k^\top + R_k,
\end{aligned}$$

η_k^f is exactly the form of $\bar{\eta}_k$, and should be used to calculate adaptive fading factors, namely,

$$\tilde{\boldsymbol{C}}_{0,k}^{f} = \frac{1}{n_w - 1} \sum_{i=k-n_w+1}^{k} \eta_i^f (\eta_i^f)^\top = \tilde{\bar{\boldsymbol{C}}}_{0,k}^{f}$$

Optimality Criterion for Adaptive TSKF

Recall Equation (4.18), (4.6), and the followings can be obtained:

$$\begin{aligned}
&\bar{\lambda}_k \bar{P}_{k|k-1} \bar{C}_k^\top - \bar{K}_k \tilde{\bar{\boldsymbol{C}}}_{0,k} \\
&\qquad = \bar{\lambda}_k \bar{P}_{k|k-1} \bar{C}_k^\top - \bar{\lambda}_k \bar{P}_{k|k-1} \bar{C}_k^\top (\bar{\lambda}_k \bar{C}_k \bar{P}_{k|k-1} \bar{C}_k^\top + R_k)^{-1} \tilde{\boldsymbol{C}}_{0,k}^{f} \\
&\qquad = \bar{\lambda}_k \bar{P}_{k|k-1} \bar{C}_k^\top \left[\boldsymbol{I} - (\bar{\lambda}_k \bar{C}_k \bar{P}_{k|k-1} \bar{C}_k^\top + R_k)^{-1} \tilde{\boldsymbol{C}}_{0,k}^{f} \right] \\
&\qquad = 0.
\end{aligned}$$

Due to $\bar{C}_k^\top$ is full column rank by default (measurement number is smaller than state number),

$$\begin{aligned}
\text{Equation (4.18)} \quad &\Leftrightarrow \quad \boldsymbol{I} - (\bar{\lambda}_k \bar{C}_k \bar{P}_{k|k-1} \bar{C}_k^\top + R_k)^{-1} \tilde{\boldsymbol{C}}_{0,k}^{f} = 0 \\
&\Leftrightarrow \quad \bar{\lambda}_k (\boldsymbol{C}_{0,k}^{f} - R_k) = \tilde{\boldsymbol{C}}_{0,k}^{f} - R_k \\
&\Leftrightarrow \quad \bar{\lambda}_k (C_k P_{k|k-1}^{x} C_k^\top + S_k P_{k|k-1}^{f} S_k^\top) = \tilde{\boldsymbol{C}}_{0,k}^{f} - R_k.
\end{aligned}$$

One-step ATSKF Algorithm

Based on the One-step AFKF algorithm proposed in [28], adaptive fading factor for *adaptive two-stage Kalman filter* (ATSKF) can be calculated as the following form:

$$\bar{\lambda}_k = \max \left\{ 1, \frac{\text{trace}[N_k]}{\text{trace}[M_k]} \right\}, \tag{4.23}$$

where

$$N_k = \tilde{\boldsymbol{C}}^f_{0,k} - R_k,$$
$$M_k = C_k P^x_{k|k-1} C_k^\top + S_k P^f_{k|k-1} S_k^\top.$$

The adaption is implemented as

$$P^x_{k|k-1} = \bar{\lambda}_k \left(A_{k-1} P^x_{k-1|k-1} A_{k-1}^\top + Q^x_{k-1} + U_k (\bar{U}_k Q^f_{k-1})^\top \right) \tag{4.24}$$
$$P^f_{k|k-1} = \bar{\lambda}_k \left(H_{k-1} P^f_{k-1|k-1} H_{k-1}^\top + Q^f_{k-1} \right). \tag{4.25}$$

4.4 Simulation Results and Conclusion

4.4.1 ASKF and Sensor Selection

In this simulation, *augmented-state Kalman filter* performance and its sensor selection have been studied, in comparison with previous chapter, where fault-free model is used.

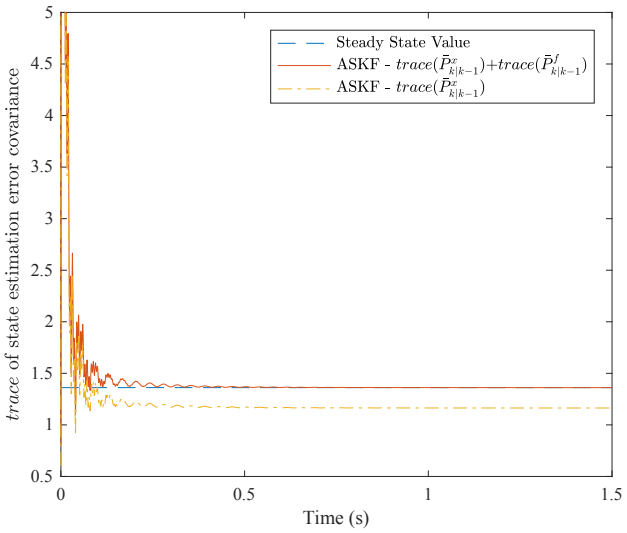

Figure 4.1: Trace of ASKF state estimation error covariance

Figure 4.1 demonstrates the trace of state estimation error covariance of the augmented system when reference measurement model is applied; compared to Figure 3.2, ASKF has larger trace value of P^x; this is because stochastic fault dynamic augmented into the system will increase the mean squared error of original system state estimation. This indicates

that more sensors will be required to achieve the same level of state estimation quality as fault-free system. Sensor selection result of the augmented state system under complex sensor type is presented in Figure 4.2. It can be observed that, in Figure 3.5, only two sets of sensors are required to outperform reference model; while in Figure 4.2, five sets are required. Therefore, it can be concluded that as system dimension increases, sensor selection algorithm will be forced to select more sensors to maintain certain estimation performance requirement.

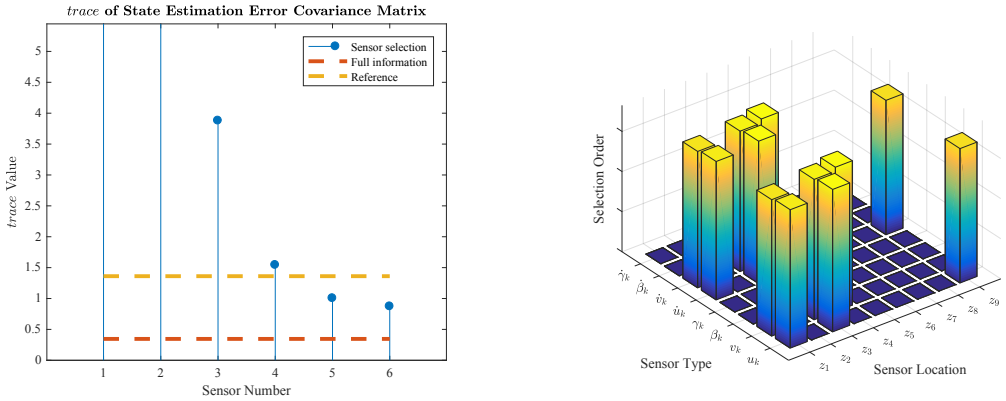

Figure 4.2: Sensor selection for augmented state system model using complex sensors.

4.4.2 OTSKF Estimation Performance

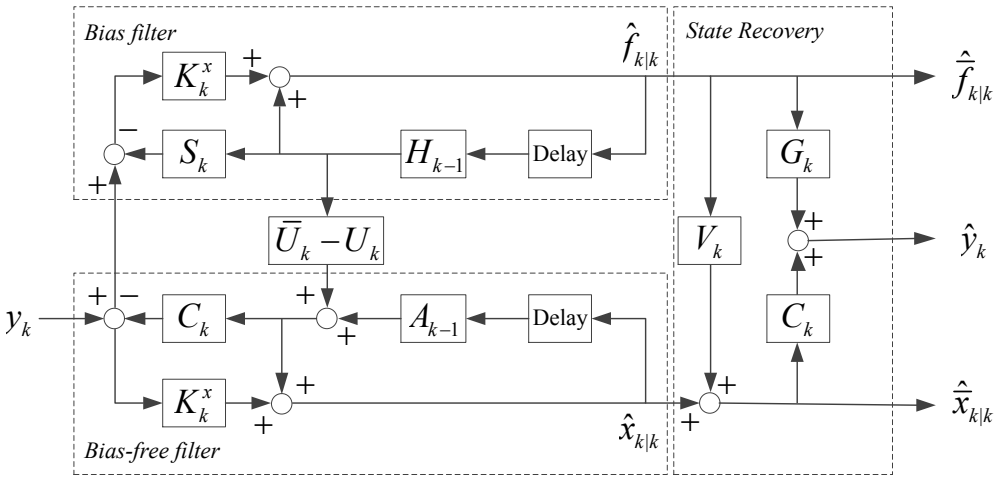

Figure 4.3: OTSKF simulation structure diagram.

The simulation structure for OTSKF is outlined in Figure 4.3. The model is designed following Equations (4.7 - 4.14) and system model in Equation (4.3). In order to demonstrate the equivalence between ASKF and OTSKF, Figure 4.4 has compared the trace value of *a priori* error covariance between ASKF and OTSKF. The almost perfect overlapping of the two functions indicates the equivalence between the two filters.

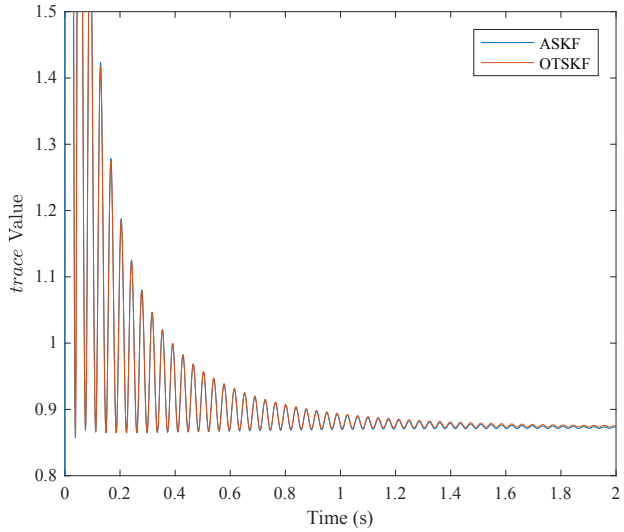

Figure 4.4: Comparison of trace values of *a priori* error covariance matrices between ASKF and OTSKF.

Estimation using Measurements under general Harmonic Imbalance Fault

Output tracking using measurement model described in Figure 4.2 is illustrated in Figure 4.5. Kalman filtering succeeded in tracking fault-free outputs; however, once fault occurs, the filter tends to track the faulty data, and visible increment of vibration magnitude can be observed from Node 3 (y_3 and y_4) and Node 4 (y_5). According to Equation (4.23), $\bar{\lambda}_k$ value is expected to reflect occurrence of sudden abnormal dynamics. During normal operation condition, $\bar{\lambda}_k$ value is 1, which indicates the conventional *Kalman filter* is maintaining adequate tracking performance; once the value becomes larger than 1, it can be concluded that the system is under dynamic changes, other modeled or unmodeled. Figure 4.6 presents the monitoring of $\bar{\lambda}_k$ changes in OTSKF, and the occurrence of f_k dynamic change is well captured after a short delay due to the windowing parameter n_w applied in actual innovation covariance. The fault estimation performance of OTSKF is shown in

Figure 4.7. and no significant fault signal is estimated.

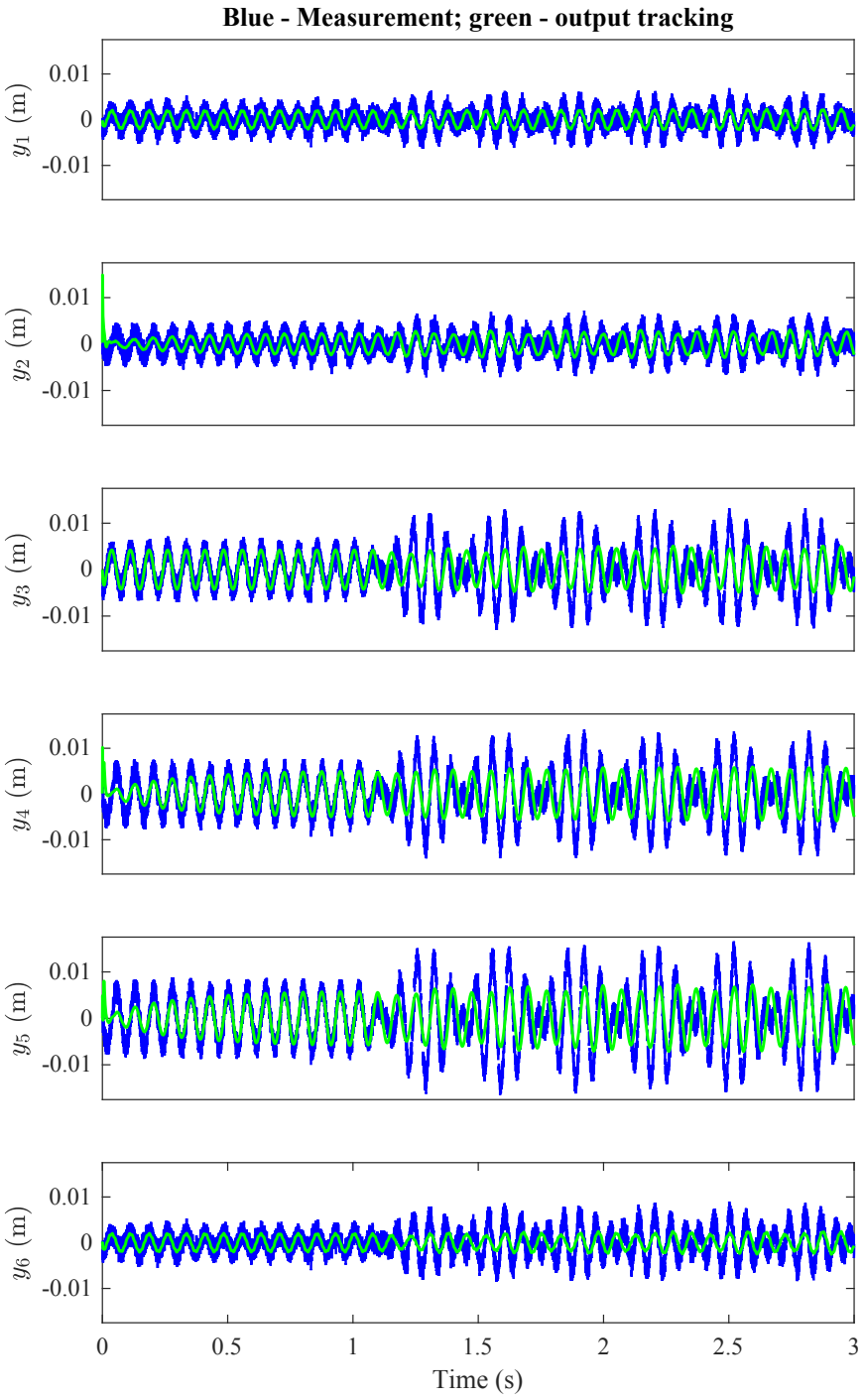

Figure 4.5: OTSKF output tracking under general harmonic imbalance fault scenario.

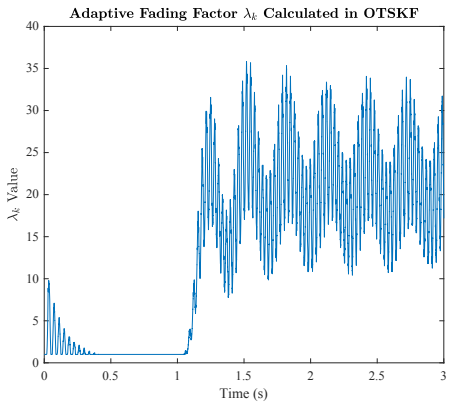

Figure 4.6: OTSKF output tracking performance indicator under general harmonic imbalance fault scenario.

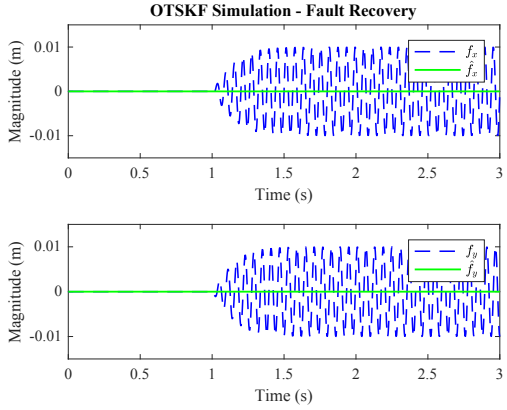

Figure 4.7: General harmonic imbalance fault estimation result via OTSKF.

Estimation using Measurements from Steady-state Imbalance Fault Response

The simulation results using the steady-state response under imbalance fault are presented in Figure 4.8, 4.9 and 4.10. As is demonstrated, when the simulation starts, the estimation algorithm intends to tract the output; however, due the the slow tracking performance, which can be observed from the phase difference between estimate and actual measurements, the output tracking eventually fails because of the filter degradation issue, and the filter failed to provide estimate for the imbalance fault.

This observation indicates that, even when there is no fault occurrence dynamics, if the simultaneous state and fault estimation algorithm fail to fast track the output, there is

no guarantee that state and fault will be successfully estimated. In this case, fast output tracking strategy is required.

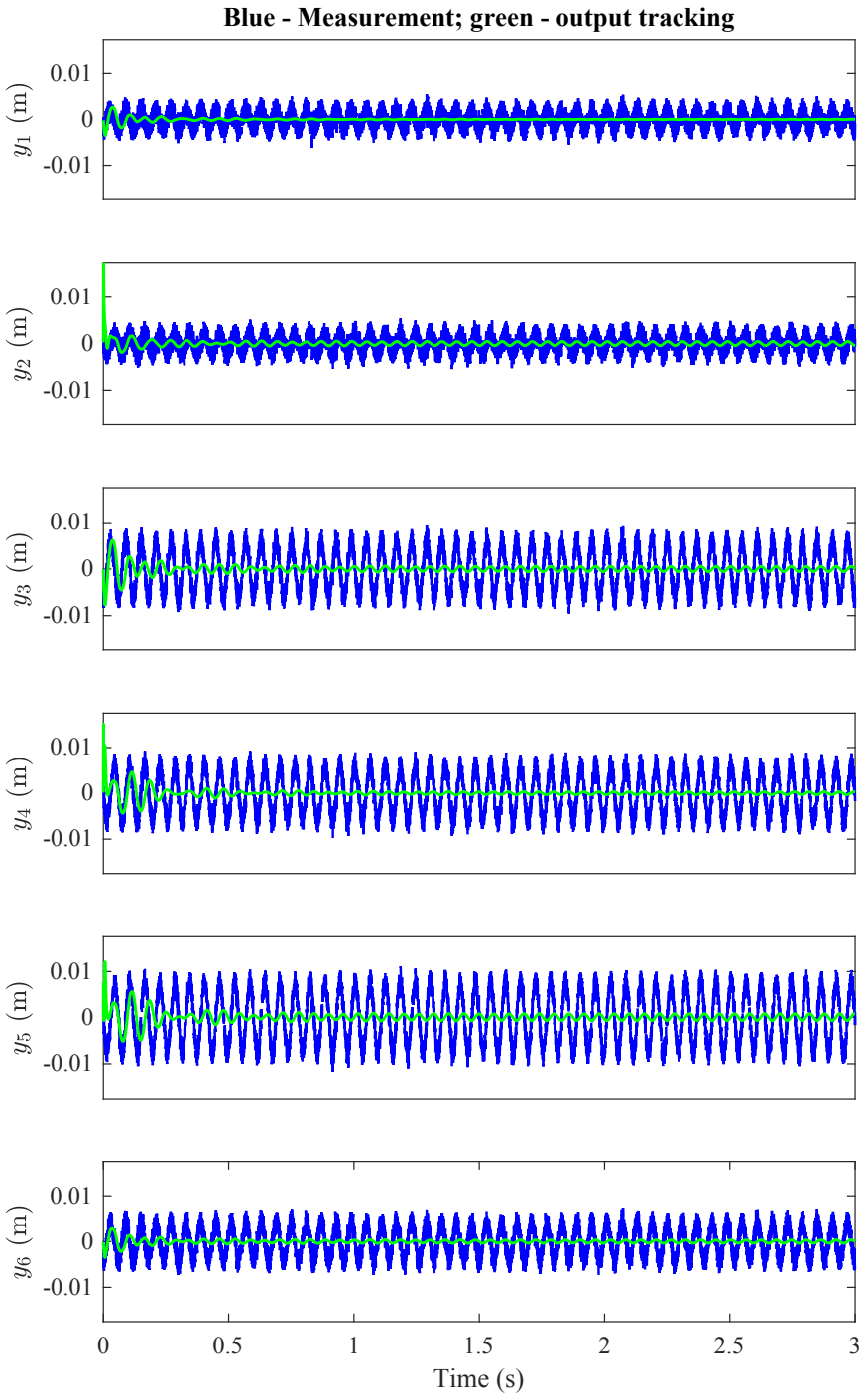

Figure 4.8: OTSKF output tracking under steady-state imbalance fault response.

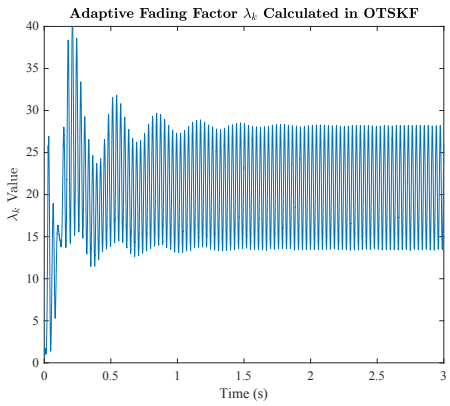

Figure 4.9: OTSKF output tracking performance indicator under steady-state imbalance fault response.

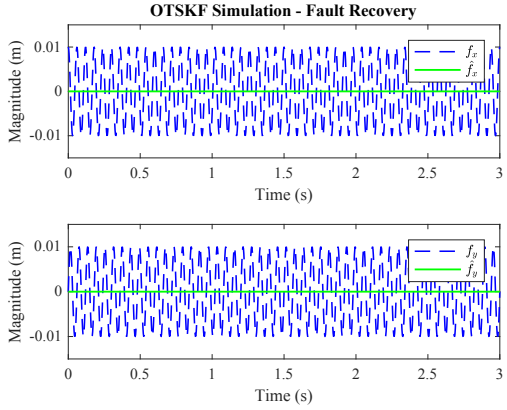

Figure 4.10: Imbalance fault estimation result via OTSKF.

4.4.3 Output Tracking using Adaptive TSKF

Estimation using Measurements under general Harmonic Imbalance Fault

Adaption is automatically added into estimation error covariance dynamics once abnormality is detected through $\bar{\lambda_k}$ following Equation (4.24) and (4.25). ATSKF output tracking and fault estimation are presented in Figure 4.11 and 4.13. As is demonstrated, the adaption applied is very effective, and satisfactory estimation result is achieved. Note that the fault comparison is made based on Equation (2.16) and (2.18) as following: the estimated $\hat{f}_k$ is first recovered into $\hat{f}_{\text{im}}$ according to Equation (2.16), and then scaled with $\omega^2 \cdot m_d$,

and eventually compared with same scaled real fault signal. This comparison is acceptable since model accuracy assumption has been made.

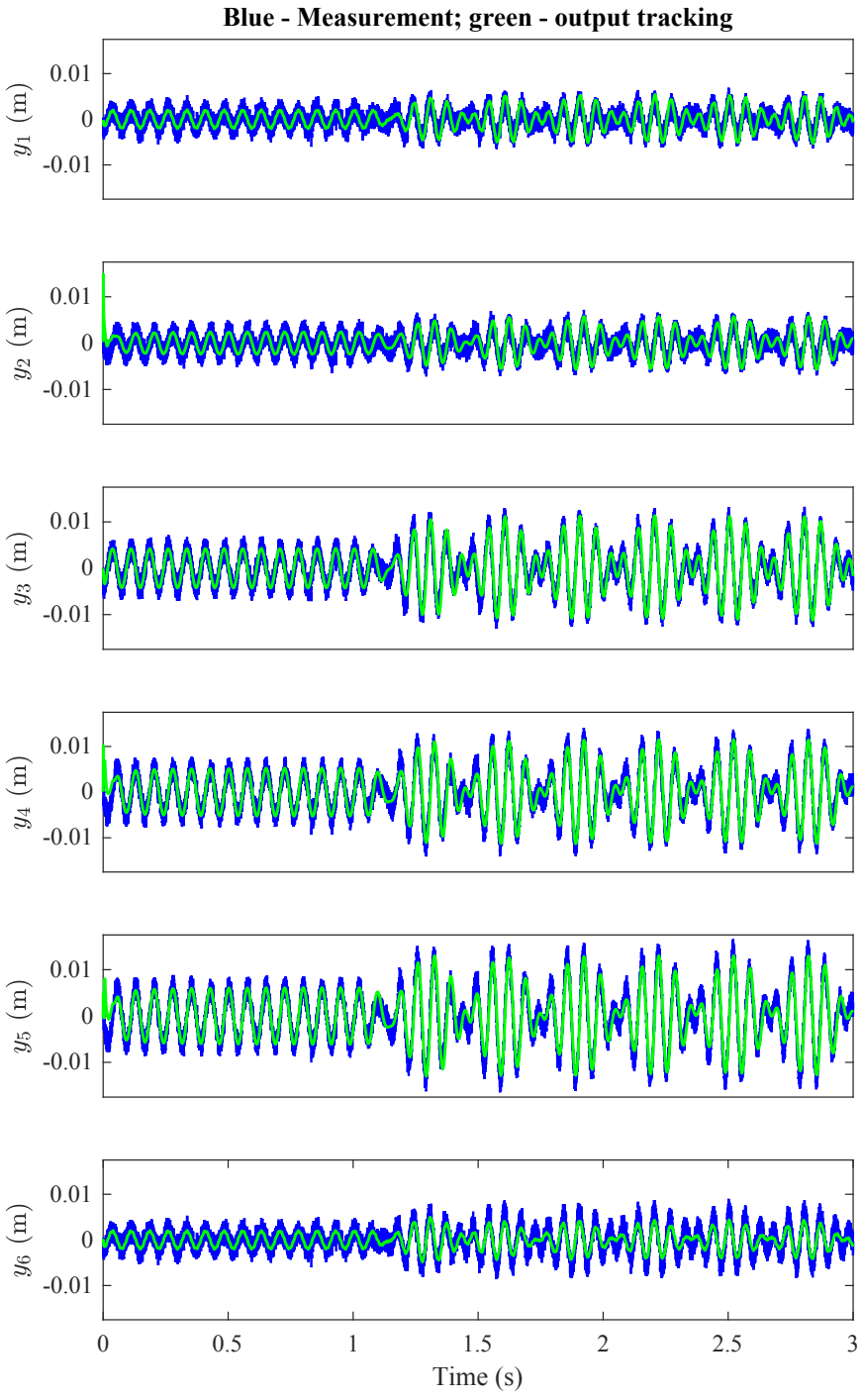

Figure 4.11: ATSKF output tracking under general harmonic imbalance fault scenario.

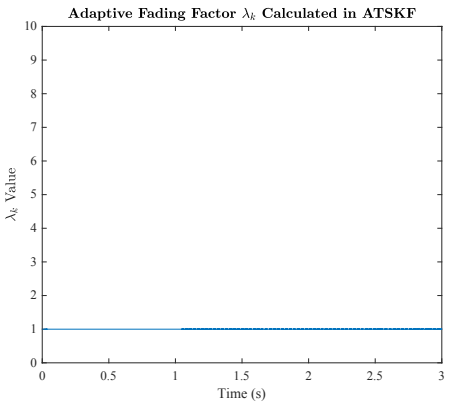

Figure 4.12: ATSKF output tracking performance indicator under general harmonic imbalance fault scenario.

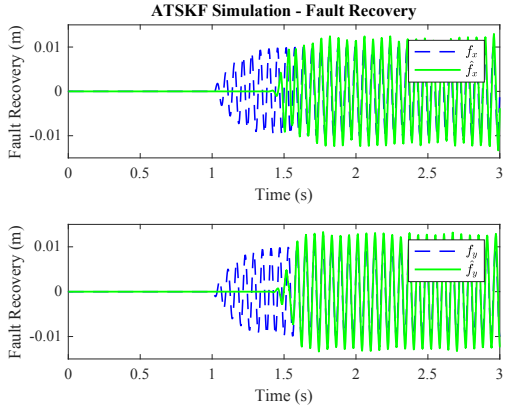

Figure 4.13: General harmonic imbalance fault estimation result via ATSKF.

Estimation using Measurements from Steady-state Imbalance Fault Response

The simulation results using the steady-state response under imbalance fault are presented in Figure 4.14, 4.15 and 4.16. As is demonstrated, the fast output tracking is achieved using the adaptive algorithm, and thus, the fault signal is eventually estimated. Simultaneous state and fault estimation is successfully achieved.

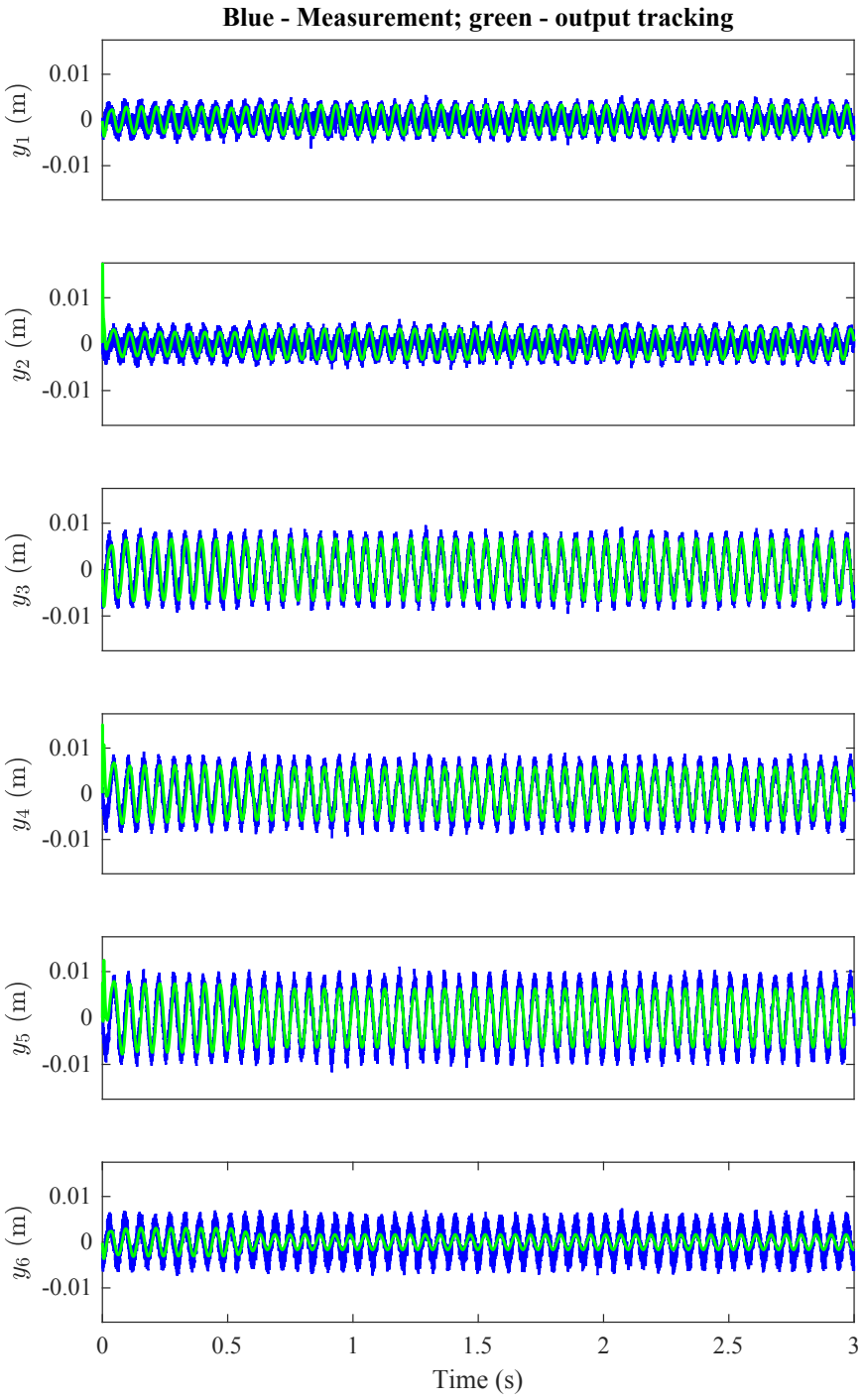

Figure 4.14: ATSKF output tracking under steady-state imbalance fault response.

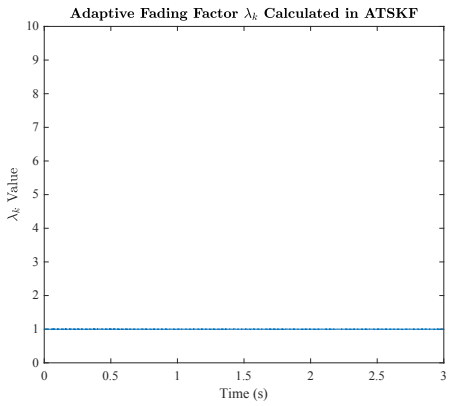

Figure 4.15: ATSKF output tracking performance indicator under steady-state imbalance fault response.

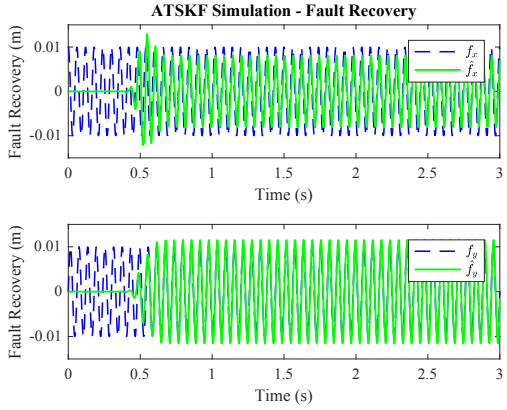

Figure 4.16: Imbalance fault estimation result via ATSKF.

4.4.4 Conclusion

In this chapter, *optimal two-stage Kalman filter* is firstly studied for easing the computation complexity of its equivalence, *augmented-state Kalman filter*, where state and fault can be simultaneously estimated; the equivalence has been presented by comparing the state estimation error covariance dynamics of both filters. Sensor selection result from the higher order augmented state system representation shows that more sensors are required for this case to maintain same level of estimation performance on fault-free system. In order to overcome the degradation of conventional Kalman filtering in real implementations, optimal adaptive approach is then studied within *two-stage Kalman filter* structure, aiming

at deriving the equivalent form of *optimal adaptive fading Kalman filter* for the augmented state system. Simulation results have demonstrate the effectiveness of this approach when handling occurrence of faults during operation.

Chapter 5

Conclusions and Future Work

5.1 Conclusions

In this thesis, state and imbalance fault estimation of a simple rotor-bearing system is studied using Kalman filtering techniques.

Firstly, finite element discretization is applied to spatially discretize a set of coupled partial differential equations that describe the motion of a simple rotor-bearing system. Both free and forced lateral responses demonstrate proper behavior of the selected model. A second-order Simulink model is then designed to perform system simulation and generate measurements.

In order to optimally and systematically choose among the large number of approximate ODE model states to measure for state estimation purpose, optimization-based sensor selection problem for Kalman filtering is investigated and an approximation algorithm is outlined for implementation. Simulation results using different covariance metrics and different sensor limitations are presented. A few fundamental limitations with respect to sensor selection for optimal Kalman filtering is then concluded based on the simulation results. Insights and guidance of sensor selection for the rotor-bearing system are analyzed.

Given the fact that a measurement model can be optimally chosen for Kalman filtering, *augmented-state Kalman filter* is then studied for simultaneous state and fault estimation of simple rotor-bearing system. *Optimal two-stage Kalman filter* is then introduced to handle some practical limitations of ASKF. Adaptive fading algorithm for OTSKF is further designed by deriving the equivalent form of *adaptive fading Kalman filter* for augmented state system. Simulations on simple rotor-bearing system model have demonstrated the effectiveness of the ATSKF on state and imbalance fault estimation.

5.2 Future Work

This research topic was proposed for a physical rotor-bearing system setup [19] from Control and Diagnosis Group, led by Dr. Qing Zhao. Unfortunately, due to some practical limitations, this thesis has ended up in more idealized simulation fashion. However, the methodologies reviewed in this thesis and some simulation results can be used in future implementation in the physical structure.

Moreover, the following topics can be further explored:

- **Practical implementation of sensor selection**: As mentioned in this thesis, Fisher Information Matrix based selection technique is perfect for sensor pre-filtering. More specifically, among tens and hundreds of states of approximate ODE model, direct exhaust search for sensors for optimal Kalman filtering is not practical. Incorporating the FIM based approach to first trim the size of feasible sensor set is advantageous for implementation.

- **Dynamic imbalance fault estimation**: Dynamic fault estimation has not been addressed in this thesis. However, since OTSKF is easily expandable, state estimation algorithms for more complicated imbalance fault scenario should be studied within this framework.

- **Sensor selection under system uncertainties**: Sensor selection for optimal Kalman filtering highly relies on accurate system model representation. Quantitative or qualitative analysis on how model uncertainty, especially fault dynamics modeling error, will affect state estimation error covariance based optimal sensor selection is of great practical value.

- **Sensor selection for optimal two-stage Kalman filter**: Since the main motivation of introducing OTSKF is to ease computation for implementation, sensor selection for OTSKF should be preferably performed within the lower order normal system and fault dynamics. Effective approaches for optimal sensor selection for simultaneous state and fault estimation should be designed.

Bibliography

[1] B. K. Aliyu, C. A. Osheku, L. M. A. Adetoro, and A. A. Funmilayo. Optimal solution to matrix Riccati equation – for Kalman filter implementation. In Vasilios N. Katsikis, editor, *MATLAB - A Fundamental Tool for Scientific Computing and Engineering Applications - Volume 3*, chapter 04. InTech, Rijeka, 2012.

[2] A. T. Alouani, P. Xia, T. R. Rice, and W. D. Blair. On the optimality of two-stage state estimation in the presence of random bias. *IEEE Transactions on Automatic Control*, 38(8):1279–1283, Aug 1993.

[3] H. T. Banks and K. L. Rehm. Experimental design for distributed parameter vector systems. *Applied Mathematics Letters*, 26(1):10 – 14, 2013.

[4] O. Y. Bas, B. Shafai, and S. P. Linder. Design of optimal gains for the proportional integral Kalman filter with application to single particle tracking. In *Proceedings of the 38th IEEE Conference on Decision and Control (Cat. No.99CH36304)*, volume 5, pages 4567–4571 vol.5, 1999.

[5] S. Edwards, A. W. Lees, and M. I. Friswell. Fault diagnosis of rotating machinery. *Shock and Vibration Digest*, 30(1):4–13, 1998.

[6] B. Friedland. Treatment of bias in recursive filtering. *IEEE Transactions on Automatic Control*, 14(4):359–367, August 1969.

[7] M. I. Friswell. Candidate reduced order models for structural parameter estimation. *ASME, Transactions, Journal of Vibration and Acoustics*, 112:93–97, 1990.

[8] M. I. Friswell, J. E. T. Penny, S. D. Garvey, and A. W. Lees. *Dynamics of rotating machines*. Cambridge University Press.

[9] E. M. Hernandez. Optimal model-based state estimation in mechanical and structural systems. *Structural Control and Health Monitoring*, 20(4):532–543, 2013.

[10] E. M. Hernandez. Efficient sensor placement for state estimation in structural dynamics. *Mechanical Systems and Signal Processing*, 85:789 – 800, 2017.

[11] C. Hsieh and F. Chen. Optimal solution of the two-stage Kalman estimator. *IEEE Transactions on Automatic Control*, 44(1):194–199, Jan 1999.

[12] J. Huddle and D. Wismer. Degradation of linear filter performance due to modeling error. *IEEE Transactions on Automatic Control*, 13(4):421–423, Aug 1968.

[13] M. B. Ignagni. Separate bias Kalman estimator with bias state noise. *IEEE Transactions on Automatic Control*, 35(3):338–341, Mar 1990.

[14] S. T. Jawaid and S. L. Smith. Submodularity and greedy algorithms in sensor scheduling for linear dynamical systems. *Automatica*, 61:282 – 288, 2015.

[15] R. E. Kalman and R. S. Bucy. New results in linear filtering and prediction theory. *Journal of basic engineering*, 83(1):95–108, 1961.

[16] K. H. Kim, J. Lee, and C. G. Park. Adaptive two-stage Kalman filter in the presence of unknown random bias. *International Journal of Adaptive Control and Signal Processing*, 20(7):305–319, 2006.

[17] K. H. Kim, J. G. Lee, and C. G. Park. Adaptive two-stage extended Kalman filter for a fault-tolerant INS-GPS loosely coupled system. *IEEE Transactions on Aerospace and Electronic Systems*, 45(1):125–137, Jan 2009.

[18] F. L. Lewis, L. Xie, and D. Popa. *Optimal and robust estimation: with an introduction to stochastic control theory*, volume 29. CRC press, 2007.

[19] G. Li, R. Pan, and Q. Zhao. Robust imbalance fault estimation of a flexible rotor system. In *2016 American Control Conference (ACC)*, pages 6703–6708, July 2016.

[20] K. Lo, Q. Lu, and W. H. Kwon. Comments on "optimal solution of the two-stage Kalman estimator". *IEEE Transactions on Automatic Control*, 47(1):198–199, Jan 2002.

[21] M. Meo and G. Zumpano. On the optimal sensor placement techniques for a bridge structure. *Engineering Structures*, 27(10):1488 – 1497, 2005.

[22] H. D. Nelson and J. M. McVaugh. The dynamics of rotor-bearing systems using finite elements. *Journal of Engineering for Industry*, 98(2):593–600, 1976.

[23] A. Olshevsky. Minimal controllability problems. *IEEE Transactions on Control of Network Systems*, 1(3):249–258, Sept 2014.

[24] S. S. Rao and F. F. Yap. *Mechanical vibrations*, volume 4. Prentice Hall Upper Saddle River, 2011.

[25] J. Rübel. *Vibrations in Nonlinear Rotordynamics-Modelling, Simulation, and Analysis*. PhD thesis, 2009.

[26] V. Tzoumas, A. Jadbabaie, and G. J. Pappas. Sensor placement for optimal Kalman filtering: Fundamental limits, submodularity, and algorithms. In *2016 American Control Conference (ACC)*, pages 191–196, July 2016.

[27] H. Waller and R. Schmidt. The application of state observers in structural dynamics. *Mechanical Systems and Signal Processing*, 4(3):195 – 213, 1990.

[28] Q. Xia, M. Rao, Y. Ying, and X. Shen. Adaptive fading Kalman filter with an application. *Automatica*, 30(8):1333 – 1338, 1994.

[29] H. Zhang, R. Ayoub, and S. Sundaram. Sensor selection for Kalman filtering of linear dynamical systems: Complexity, limitations and greedy algorithms. *Automatica*, 78:202 – 210, 2017.